

Nanoscale

Accepted Manuscript



This is an *Accepted Manuscript*, which has been through the Royal Society of Chemistry peer review process and has been accepted for publication.

Accepted Manuscripts are published online shortly after acceptance, before technical editing, formatting and proof reading. Using this free service, authors can make their results available to the community, in citable form, before we publish the edited article. We will replace this *Accepted Manuscript* with the edited and formatted *Advance Article* as soon as it is available.

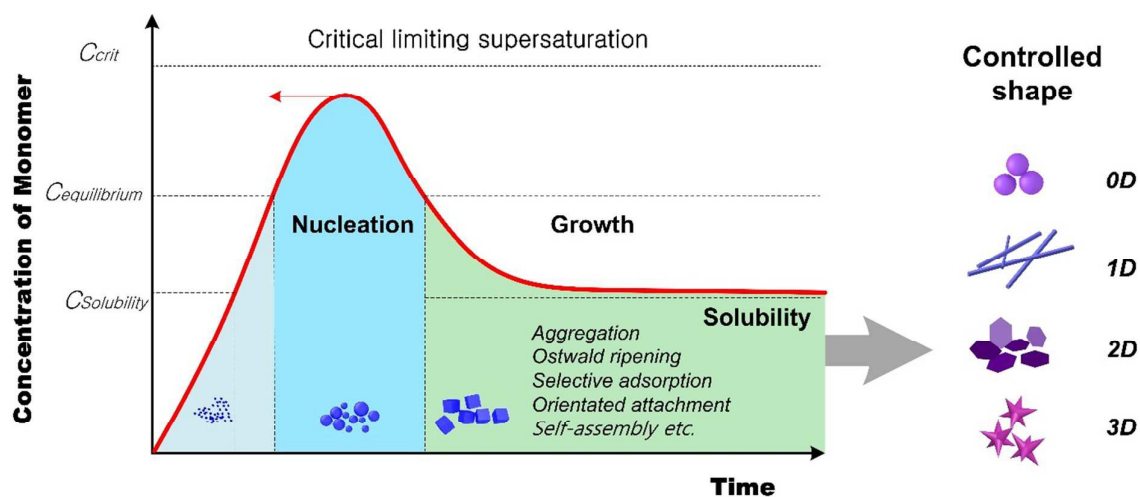
You can find more information about *Accepted Manuscripts* in the [Information for Authors](#).

Please note that technical editing may introduce minor changes to the text and/or graphics, which may alter content. The journal's standard [Terms & Conditions](#) and the [Ethical guidelines](#) still apply. In no event shall the Royal Society of Chemistry be held responsible for any errors or omissions in this *Accepted Manuscript* or any consequences arising from the use of any information it contains.

TOC

Shape control of inorganic nanoparticles from solution

Zhaohui Wu, Shuanglei Yang, Wei Wu *



The controlled shapes of inorganic nanoparticles through diverse mechanisms from solution was elucidated based on classical nucleation and growth theory

Shape control of inorganic nanoparticles from solution

Zhaohui Wu^{a, b}, Shuanglei Yang^{b, c}, Wei Wu^{b, d} *

^a Department of Chemical Engineering, Kyung Hee University, Seocheon-Dong, Giheung-Gu, 446-701 Yongin-Si, Korea

^b Laboratory of Printable Functional Nanomaterials and Printed Electronics, School of Printing and Packaging, Wuhan University, Wuhan 430072, P. R. China

^c College of Chemical and Environmental Engineering, Qingdao University, Qingdao, P. R. China

^d Department of Physics and Materials Science, City University of Hong Kong, Hong Kong SAR, P. R. China

Corresponding authors: weiwu@whu.edu.cn (W. Wu)

Abstract

The inorganic materials with controllable shape have been a intensely subject in nanoscience over the past decades. Controlling over novel and anisotropic shape of inorganic nanomaterials differing from bulk materials enables their unique and tunable properties for widespread applications such as biomedicine, catalysis, fuel or solar cell and magnetic data storage. This review presents a comprehensive overview in shape-controlled inorganic nanomaterials through nucleation and growth theory and experimental conditions controlling (including supersaturation, temperature, surfactants and secondary nucleation), providing a brief account of shape control of inorganic nanoparticle during wet-chemistry synthesis process. Subsequently, typical mechanisms for shape-controlled inorganic nanoparticles and general formed shape of nanoparticles by each mechanism are also expounded. Furthermore, the difference of similar mechanisms for shape controlling of inorganic nanoparticles are also clearly described. The authors envision this review providing valuable guidance on experimental conditions and process control for tunable shape of inorganic nanoparticles in solution state.

34	Content	
35	Abstract.....	2
36	1 Introduction.....	4
37	2 Nucleation and growth theory.....	6
38	2.1 Classical nucleation.....	6
39	2.2 Classical growth and dissolution.....	8
40	2.3 Conventional factors on shape control.....	10
41	2.3.1 Supersaturation.....	10
42	2.3.2 Temperature.....	14
43	2.3.3 Seeds and templates.....	15
44	2.3.4 Surfactants or additives.....	16
45	3 The shape-controlled mechanisms.....	18
46	3.1 Adsorption growth and underpotential deposition.....	19
47	3.2 Agglomeration and aggregation.....	21
48	3.3 Orientation attachment and self-assembly.....	22
49	3.4 Ostwald ripening.....	24
50	4 The prospects and outlook.....	26
51		

52 **1 Introduction**

53 Nanomaterials, especially inorganic nanomaterials (such as metal, metal oxide, metal sulfate, quantum
54 dots, et al.) with fundamental properties have attracted considerable interest in developing
55 biomedicine, catalysis, fuel cell, sensors and magnetic data storage.¹⁻⁷ Over last two or three decades,
56 much progress has been pursued for synthesis of diverse inorganic nanomaterials and exploring their
57 revolutionary applications. General agreement for synthesis of inorganic nanomaterials have been
58 made that the synthesis can be carried out in two essential approaches, referring as “bottom-up” and
59 “top-down”.⁵ The top-down approach is based on physical and lithographic principle of micro- and
60 nanotechnology and started from a large material entity, then the produced inorganic nanoparticles
61 (NPs) with size in medium to lower nanometer range but with a relative broad size distribution and
62 uncontrollable shape. Inversely, bottom-up approach, ionic, atomic, or molecular units are assembled
63 through various reaction processes to form structures in nanometer range and provides high structural
64 purity inorganic NPs with diverse shape, size, composition and surface properties. From the
65 fundamental and functional viewpoints, the bottom-up approach is far more popular in synthesis of
66 inorganic NPs and is considered as promising route to control the constitute, growth, final nano-entity
67 morphology and properties of inorganic NPs.⁸⁻¹⁰ In solution state, the bottom-up synthesis route for
68 various shape-controlled inorganic NPs can be facilitated in precipitated methods, preformed-seed-
69 mediated growth method (such as noble metal, oxide), polyol approach, template approach,
70 electrochemical synthesis and photochemical synthesis routes.¹¹⁻¹³

71 Inorganic NPs obtained from bottom-up route in solution state originates from the fact that the
72 tunable novel properties of inorganic NPs could be drastically altered in their dimensional shape. In
73 dimensional range of inorganic NPs, shape can be classified into 0D (isotropic structure), 1D, 2D, and
74 3D (anisotropic structure). The typical solid and mesoporous/hollow shape of inorganic NPs based on
75 dimensionality, is shown in **Figure 1**. In case of 0D inorganic NPs, typical shapes include spherical,
76 pseudo-spherical, dodecahedral, tetrahedral, octahedral, cubic, and corresponding hollow structure
77 morphologies. 1D morphology of inorganic NPs are nanotubes, nanoneedle, nanorods or nanowires,

78 nanoshuttles, nanocapsule and hollow structures etc.¹⁴⁻¹⁵ Round disk, hexagonal/ triangular/
79 quadrangular plates or sheets, belts, mesoporous- hollow nanosphere, hollow rings, etc. belong to 2D
80 shape of inorganic NPs.¹⁶ 3D morphology of inorganic NPs is complex one, including nanourchins,
81 nanoflowers, nanostar, polygonal nanoframes, multiple hollow shelled NPs, hollow bunches and so
82 on.¹⁷⁻¹⁸ Comparing with the simple isotropic morphology of inorganic NPs, novel anisotropic
83 morphologies of inorganic NPs give rise to new features and unique physicochemical properties due
84 to the number of their step edges, kink sites on surface and high surface-area-to volume ratio in
85 nanoscale regime. For instance, polyhedral Au NPs with high-index facets exhibit excellent optical
86 and catalytic properties,^{12, 19} Au rod with different ratios of length and width display different
87 transverse and longitudinal plasmon bands for surface-enhanced Raman scattering and biomedicine,
88 ²⁰⁻²¹ and branched Au NPs with multiple tips (such as, stars, flowers) ²²⁻²³ have been attracted
89 increasing interest in catalysis, surface-enhanced Raman scattering, and sensing.²⁴⁻²⁵ A great deal of
90 effort has been devoted to control over shape of inorganic NPs, and much progress in synthesis of
91 shape-controlled inorganic NPs and corresponding shape-dependent properties have been made over
92 last decades.²⁶⁻²⁷ Generally, the shape formation of inorganic NPs can be controlled or varied by
93 thermodynamically or kinetically controlling manner during solution state. Normally,
94 thermodynamic controlled morphology of inorganic NPs was produced, when the reaction is driven
95 by chemical potential of reaction solution, which is directly related with temperature and
96 supersaturation of solution. Kinetically controlled different dimension morphologies can be obtained
97 by altering the reaction conditions, which happens when freshly produced atoms are in rapid collision
98 with smaller number of embryos in local regions of high supersaturation for the formation of nuclei,
99 according to the nucleation theory. And then the growth of nuclei with kinetic controlled process
100 contributes to the formation of nanoparticles with anisotropic shape.¹¹ Thus, the synergistic effects of
101 thermodynamic and kinetic aspects are considered as critical roles in determining the final shape of
102 inorganic NPs.²⁴

103 Recently, most viewpoints and efforts in the literatures are focused on the effect of adjusting
104 reaction parameters on size and shape evolution in capping molecule-assisted synthesis and other

105 innovative synthesis approaches.²⁸⁻³⁰ Although, it is worth noting that there are no simple rules to
106 determine the final shape of inorganic nanomaterials. The basic principle of nucleation and growth
107 that typically occurs in the bulk solution throughout all the reactions, and corresponding altered
108 reaction parameters including precursor concentration or supersaturation, reaction temperature/aging
109 time and additives still have not been paid attention. Thus, to address a comprehensive understanding
110 of the formation mechanism and shape evolution policies of inorganic nanomaterials, the influences
111 of these reaction parameters during synthesis process of inorganic nanomaterials are studied. Then,
112 the typical mechanisms for shape-controlled inorganic NPs also have been presented for guidance of
113 further studies.

114 **2 Nucleation and growth theory**

115 **2.1 Classical nucleation**

116 The definition and classification of nucleation have been described by Mullin since 1961,³¹ in which
117 nucleation is a process whereby second phase generated from one phase. In solution state, that is,
118 solid particles are considered as second phase generated from precursors solution phase by nucleation
119 process. Here, if the solid nuclei generated from homogenous supersaturated bulk solution is referred
120 as primary nucleation. Inversely, if the fresh nuclei generated in a supersaturated bulk solution in
121 presence of other particles or materials with same and different components (such as, container
122 surfaces, impurities, grain boundaries, dislocations), is named as “secondary nucleation” and
123 “heterogeneous nucleation”, respectively. Additionally, occurrence of heterogeneous nucleation and
124 secondary nucleation is much easier than primary nucleation due to low energy barrier, since stable
125 nucleating sites already presented in the system. As presented by Mullin,³¹ and other researches,^{11,32}
126 the formation of homogeneous nuclei is considered as a thermodynamically process driving by the
127 supersaturation of bulk solution and deciding by total free energy (ΔG) of a NPs, defining as the sum
128 of surface free energy and bulk free energy ΔG_v , as shown in Eq. 1

$$129 \quad \Delta G = 4\pi r^2 \gamma - \frac{4}{3} \pi r^3 \Delta G_v \quad (1)$$

130 where r and γ is radius of particle and the surface energy, respectively. As regards of the free energy
 131 of bulk crystal ΔG_v , is defined as free energy change of transformation to unit volume of particles,
 132 dependent upon temperature T , Boltzmann's constant k_B , its molar volume v , and supersaturation ratio
 133 of bulk solution S . That is, $\Delta G_v = \frac{-2\gamma}{r} = \frac{-2k_B T \ln(S)}{v}$. Particularly, S is defined as ratio of monomer

134 concentration in solution C to equilibrium monomer concentration C^* in the crystals ($S=C/C^*$).

135 In homogeneous solution, nucleation process is accomplished by costing the increased free energy to
 136 form an interface between bulk solution and surface solid nuclei. Nuclei with formed radius are highly
 137 with respect to supersaturation level, and rapidly increase and narrow distribution of supersaturation
 138 results in small size of particles in terms of the definition of bulk free energy ΔG_v . The critical value
 139 of ΔG and critical radius of nuclei that existed in the bulk solution is conducted by differentiating ΔG
 140 with respect to radius r when ΔG is set to zero, $d(\Delta G_{crit})/dr=0$, giving a critical free energy in Eq.

141 2. Apparently, ΔG_{crit}^{homo} is required to obtain stable nuclei within solution (**Figure 2**).³³⁻³⁵ Then, the
 142 critical radius corresponds to the minimum size of nuclei surviving in solution without being
 143 redissolved, as defined in Eq. 3.

$$144 \quad \Delta G_{crit} = \frac{4}{3} \pi \gamma r_{crit}^2 = \Delta G_{crit}^{homo} \quad (2)$$

$$145 \quad r_{crit} = \frac{-2\gamma}{\Delta G_v} = \frac{2\gamma v}{k_B T \ln S} \quad (3)$$

146 A nucleation rate of nuclei N formed per unit time per unit volume, were written in a form of
 147 Arrhenius reaction velocity equation, which is commonly used for the rate of a thermally activated
 148 process:

$$149 \quad \frac{dN}{dt} = A \exp(-\Delta G_{crit} / k_B T) = A \exp\left(\frac{-16\pi\gamma^3 v^2}{3k_B^3 T^3 (\ln S)^2}\right) \quad (4)$$

150 where A is a pre-exponential factor. According to the Eq.4, the nucleation rate can be varied by the
 151 experimental parameters involving supersaturation, temperature and surface free energy, and the detail
 152 influence will be introduced in the following part. The higher concentration of monomer, high

153 temperature and lower critical energy barrier favor for rapid nucleation rate, resulting in high
154 population of nuclei with small size, as demonstrated by a large number of synthesis process.³⁶⁻³⁷
155 Additionally, some non-classical nucleation theories, such as, two-step nucleation for protein
156 crystallization, and cluster aggregation for agglomeration of particles, also were explored for
157 addressing the nucleation process.³⁸⁻³⁹

158 **2.2 Classical growth and dissolution**

159 After nucleation, subsequent growth of nuclei is strongly determined the shape of nanomaterials,
160 which is thermodynamically driven by the decreasing surface free energy of generated particles.
161 Growth process involves deposition of elementary (including atoms, molecules, assemblies or
162 particles) attaching on performed NPs in a growth medium (plasma, melt, solution, gel, etc.). And this
163 attachment occurs at sites of nuclei surface. The density of existed sites on performed nuclei surface
164 together with the kinetics of incorporation into these sites are crucial roles to determine the growth
165 rate of NPs.⁴⁰ In classical growth theory, there are two growth mechanisms including surface reaction
166 and monomer's diffusion to particle surface.⁴¹

167 As described by Fick's first law of diffusion, if the monomers flux passing through a surface of
168 spherical NPs with radius x , the diffusion rate of monomers through its surface can be written as

$$169 \quad \frac{dm}{dt} = JA = -4\pi x^2 D \frac{dC}{dx} \quad (5)$$

170 where J is monomer flux and D is diffusion constant. The diffusion rate of monomers at spherical NPs
171 surface with radius r at steady state, the above equation can be written as

$$172 \quad \frac{dm}{dt} = 4\pi r D (C_b - C_i) \quad (6)$$

173 where C_b is concentration of monomers within bulk solution, C_i is concentration of monomers at
174 interface of solid/ liquid. Similarly, equations can be written for the rate of surface reaction,

$$175 \quad \frac{dm}{dt} = 4\pi r^2 k (C_i - C_r) \quad (7)$$

176 where k is mass transfer coefficient, C_r is the equilibrium concentration of solid NPs. If the diffusion
177 is the limiting factor and particle size changes with time, the diffusion of monomers onto the surface
178 of NPs is given in equation (8). Similarly, if the surface reaction is the limiting factor, the equation (7)
179 can be described in (9).

$$180 \quad \frac{dr}{dt} = \frac{D\nu}{r} (C_b - C_r) \quad (8)$$

$$181 \quad \frac{dr}{dt} = k\nu(C_b - C_r) \quad (9)$$

182 where C_r is the solubility of the NPs, and ν is molar volume of bulk NPs. The growth of
183 nanoparticles is controlled the two limiting factors neither by diffusion nor surface reaction, and then
184 the increase in particles size with time shows in equation (10).

$$185 \quad \frac{dr}{dt} = \frac{D\nu}{r + D/k} (C_b - C_r) \quad (10)$$

186 A scheme of concentration as driving force for diffusion and reaction of crystal growth is shown in
187 **Figure 3**. Diffusion-limited or reaction-limited process with different concentration of precursor
188 monomer determines the shape of NPs by growth rate.⁴² Within solution of high concentration of
189 precursor monomer solution, growth rate is controlled by the diffusion-limited process. That is,
190 diffusion of precursor monomer is rate-determining step. Then, precursor monomers are precipitated
191 immediately onto the surface of NPs through the bulk reaction medium and solvent. Nevertheless, in
192 the case of reaction-limited growth process, when concentration of precursor monomer is low and
193 growth is greatly limited by surface reaction of monomers, total growth rate is determined by the
194 relative nucleation and growth rate of monomers on surface of NPs.

195 From equations (8) and (9), both diffusion-limited and reaction-limited growth is driving by precursor
196 monomer concentration. Then, the diffusion-limited growth or reaction-limited growth is decisive
197 factor for shape and size control of NPs. Normally, the diffusion-limited growth is desirable process
198 for production of NPs with monodispersity, but reaction-limited growth determines the final shape of
199 NPs. During the diffusion-limited growth process, organic ligands or surfactants adsorbed on the

200 surface of performed NPs introducing the diffusion barrier is a flexible and effective approach to get
201 controlled shape with monodisperse size.

202 Here, it is worth noting that the occurrence of growth is on condition of positive concentration
203 gradient between higher bulk concentration of solution and particles equilibrium concentration.

204 Whereas, dissolution of particles occurs in the case of negative concentration gradient between bulk
205 concentration of solution and higher particles equilibrium concentration as driving force. Generally,

206 dissolution of NPs is induced by temperature, pH, polymorph, size. However, the thermodynamic
207 parameter temperature has a negative effect on dissolution of inorganic NPs. Thus, the common

208 parameters for dissolution of inorganic NPs are polymorphic form, and pH change of solution.

209 Practically, varying of pH of the solution is the most direct and effective route to get dissolution of
210 inorganic NPs (such as, adding H^+ , OH^- , NH_3),⁴³⁻⁴⁵ and this principle is based on the combination

211 ability between metal ions and hydroxyl, resulting in the increased concentration of solution by
212 dissolving solid particles segment. Recently, intensive studies have been carried out in addressing

213 novel shape controlling through a growth-dissolution-recrystallization process with pH adjusting of
214 bulk solution.⁴⁶ Furthermore, the dissolution-recrystallization process also has been developed for

215 phase transformation of polymorphism of inorganic NPs with different shape,⁴⁷ and producing hollow
216 structure.⁴⁸⁻⁴⁹ For instance, 3D rhombohedral α - Fe_2O_3 have been synthesized by phase transformation

217 of initial intermediate β - $FeOOH$ nanowires through such dissolution-recrystallization process, as
218 reported by Lin and co-workers. The polynuclei but unstable β - $FeOOH$ nanowires were hydrolyzed to

219 form two-line ferrihydrite (α - Fe_2O_3) nuclei through dissolution-recrystallization of phase
220 transformation, then the formed small α - Fe_2O_3 nuclei went through mechanisms of aggregation,

221 orientation attachment and recrystallization of Ostwald ripening to form 3D rhombohedral α - Fe_2O_3
222 NPs.⁵⁰ 2D or 3D hollow α - Fe_2O_3 nanostructures with tunable shape (nanotubes, nanobeads, and

223 nanorings) with dissolution-recrystallization controlling after 48 h in hydrothermal route. The
224 formation of α - Fe_2O_3 NPs with hollow structures were obeyed on the mechanisms of nucleation,

225 aggregation, dissolution and re-crystallization successively. Further, the dissolution process occurred
226 on the (001) planes perpendicular to c-axis due to weak adsorption of phosphate ion, resulting in the

227 coordination effect between Fe^{3+} and phosphate ions to accelerate the dissolution process.⁴⁴
228 Additionally, Wu and co-workers also found that the sulfate ions also favored the dissolution of α -
229 Fe_2O_3 owing to the coordinated effect with ferric ions during synthesis process of 1D magnetic iron
230 oxide short nanotubes.⁵¹

231 **2.3 Conventional factors on shape control**

232 **2.3.1 Supersaturation**

233 Supersaturation generally is expressed as concentration difference, $\Delta C = C_b - C_r$. In a typical
234 synthesis process of inorganic NPs, although, the reaction solution contains precursor monomers,
235 reductant agents, solvent, or/and stabilizers and other additives. Supersaturation refers as precursor
236 monomer concentration or precursor monomer ratio in single or multiple precursor monomers system,
237 respectively. From the classical nucleation and growth theory, supersaturation plays a major and direct
238 role in determining nucleation and growth rate.^{28, 52} For synthesis inorganic NPs in solution state,
239 LaMer theory is a widespread accepted theory for nucleation and growth of NPs, in which the
240 nucleation and growth theory can be divided into two stages, in **Figure 4**.^{53, 54} At initial stage, free
241 monomers concentration in bulk solution increases rapidly and cross metastable zone until reach the
242 “burst nucleation” point, consuming the concentration of free monomers significantly in solution and
243 increasing the number of the solid particles rapidly. During this process, the number of nuclei and
244 concentration consuming rate are mainly dependent on nucleation rate. That is, fast nucleation rate is
245 able to decrease monomer concentration shapely and generates a huge number of nuclei rapidly. The
246 formed nuclei under the control of the diffusion of monomers also consumes monomers concentration
247 during growth period, causing the monomer concentration in the solution decrease continuously.
248 Furthermore, the aggregation/agglomeration, or Ostwald Ripening and other mechanisms may occur
249 among the performed nuclei, reducing the number of solid particles until the equilibrium state of the
250 bulk solution.⁵⁵⁻⁵⁷ During the growth process, if the generated nuclei have a tendency to form low-
251 energy NPs with supplying of sufficient energy at the bulk solution or low concentration of precursor
252 monomer under thermodynamic control, usually cause 0D spherical, pseudo-spherical, or other

253 isotropic NPs. Otherwise, the growth of nuclei driving by kinetical control forms anisotropic shape at
254 high precursor monomer concentration. In other word, supersaturation increasing rate or consuming
255 rate have strongly influence on nucleation and growth, which can be altered by concentration of
256 precursor monomer directly, coordination of solvent, chelation effect of pH.⁵⁸

257 **The concentration of precursor monomer and additives**

258 Supersaturation are directly and significantly altered by adding type of precursor monomer (injection
259 or dumping),²⁶ reductant concentration or reductant ratio,⁵⁹ coordination with other ions or agents,⁶⁰⁻
260 ⁶¹ etc. in one-pot synthesis or seed-mediated route.⁶²⁻⁶³ Particularly, reductant agents, the ratio between
261 precursor and reductant also significant parameters to control the depleting rate of precursor monomer
262 for the formation of inorganic NPs. Such as, Teranishi and co-workers have reported that progressive
263 increasing the concentration of reductant agent (ascorbic acid) in growth solution, polyhedral
264 morphologies of Au NPs were evolved from octahedral to truncated octahedral, cuboctahedral,
265 truncated cubic, cubic, and finally trisoctahedral structures as facilitated in a facile seed-mediated
266 route (**Figure 5**). The shape controlling of Au NPs by the reductant of ascorbic acid was explained in
267 terms of the the effect of exposed surface planes of Au seeds in ascorbic acid with different
268 concentration. That is, with higher concentration of ascorbic acid in growth solution, Au seeds were
269 surrounded by higher lattice planes for a face-centered-cubic structure due to rapid growth of seeds,
270 producing a thermodynamically unstable structure. Conversely, with addition of low concentration of
271 ascorbic acid, the formation of a thermodynamically stable structure was favored by precipitating a
272 small amount of atoms onto the Au seeds.⁶⁴ Additionally, the amount of seed NPs also have
273 tremendous impact on the final shape of inorganic NPs in the seed-mediated process due to surface
274 area for growth.⁶⁵

275 **pH effect**

276 Altering pH through addition of acid or alkali (H^+ , OH^- or NH_3) results in modulation state of
277 chemical species in solution and coordination bonding with ions in precursor monomer solution to
278 form complex. Eventually, promoting or postponing release rate of ions from the coordination

279 bonding for supersaturation enables adjusting the initial nucleation rate for shape controlling.⁶⁶⁻⁶⁸ This
280 general trend is obviously observed in synthesis of metal oxide or metal materials.⁶⁹⁻⁷¹ Xue and co-
281 worker have used pH-dependent precursor species $\text{Cu}(\text{OH})_2$, $\text{Cu}_2(\text{OH})_3\text{NO}_3$, and $\text{Cu}(\text{OH})_4^{2-}$ in a
282 starch reduction solution to achieve Cu_2O NPs with shape evolving from 1D nanowires to 3D
283 polyhedral. During this process, pH-dependent precursors was available to manipulate reaction
284 kinetics of reduction and complexation reactions for exquisite controlling over shape and composition
285 of Cu_2O NPs. Furthermore, high pH is of benefit to promote the reduction power of starch and
286 complexation ability of OH^- facilitated the shape evolution of Cu_2O NPs.⁷² Additionally, pH also
287 adjusts surface properties of preformed NPs and chemical or physical state of surfactants or additives,
288 leading to different adsorption mode or adsorption amount on the surface of performed NPs. As a
289 result, selective growth or aggregation/agglomeration, and self-assembly favour the shape evolution
290 of inorganic NPs.⁷³ For instance, as presented by Wang and co-workers, $\alpha\text{-Fe}_2\text{O}_3$ hierarchical
291 nanostructures including 3D houseleek-like and 2D snowflake-like dendrites were produced with
292 changing pH and different formation mechanisms, as shown in **Figure 6**. The pH changing
293 significantly affected the growth rate of $\alpha\text{-Fe}_2\text{O}_3$ by adjusting the supply of Fe^{3+} . On condition of
294 $\text{pH} \geq 6$, 2D snowflake-like $\alpha\text{-Fe}_2\text{O}_3$ dendrites were formed by the self-assembly of primary $\alpha\text{-Fe}_2\text{O}_3$
295 NPs preferentially along six crystallographically equivalent $(1\bar{1}00)$. Whereas, in the case of $\text{pH} \leq 5$,
296 3D houseleek-like $\alpha\text{-Fe}_2\text{O}_3$ NPs were generated by successively aggregation of round flakes with their
297 up and bottom surfaces parallel to (0001) plane, and continuous grew along $[0001]$ for single
298 crystalline spindle-like $\alpha\text{-Fe}_2\text{O}_3$, which continuous aggregated at each tips to form 3D houseleek-like
299 $\alpha\text{-Fe}_2\text{O}_3$ NPs.⁷⁴ Furthermore, for some inorganic nanomaterials with polymorphism, adjustment of pH
300 also promotes dissolution for phase transformation.^{46, 48-49, 75}

301 **Solvent**

302 Solvents with different functional groups (such as ionic liquid) provide special coordination between
303 precursor monomer, which is of advantageous for the formation process of inorganic NPs under
304 thermodynamic or kinetic controlling due to adjustment of supersaturation increase or depletion rate.³⁶

305 ⁷⁶⁻⁷⁷ In addition, mixture of different solvents or solvent with different components enables the shape
306 control of inorganic NPs. ⁷⁸⁻⁷⁹ Such as, Zhang and co-worker have selectively prepared magnetic
307 greigite nanosheets and NPs by altering the mixed ratio of ethylene glycol and water. That is,
308 magnetic greigite nanosheets were generated in pure ethylene glycol, and irregular NPs were obtained
309 in mixed solvents (EG +H₂O).⁸⁰ Surface-coordinating ligand or selective adsorption from solvent on
310 surface of presented NPs also helping define the monodispersity and shape of NPs have been
311 frequently explored in polyol process. ⁸¹ For instance, Schaak and co-worker added different
312 precursors including rhodium(II) trifluoroacetate dimer [Rh₂(TFA)₄], rhodium bromide (RhBr₃), and
313 rhodium chloride (RhCl₃) into the polyol solvents ethylene glycol (EG), diethylene glycol (DEG),
314 triethylene glycol (TREG), and tetraethylene glycol (TEG) individually to yield different shape of Rh
315 NPs, as shown in **Figure 7**. Such as, when using precursor RhBr₃, Rh truncated cube was produced in
316 EG, Rh cube with the highest quality was formed in DEG, but produced concave cube, mixed concave
317 and branched morphology were appeared in TEG. The reasonable explanation for shape evolution of
318 Rh NPs by using different solvents is surface-adsorbing species, basing on each polyol solvent with
319 only changed anion. ⁸²

320 **2.3.2 Temperature**

321 From classical nucleation and growth theory, temperature is a thermodynamic parameter of reaction
322 solution. High temperature indicating energetic movement of molecules and ions, cause instability of
323 reaction solution due to high Gibbs free energy. In reacted solution for synthesis of inorganic NPs,
324 such increasing temperature of reaction causes supersaturation increase rate or reduction rate of
325 precursor monomer in solution increasing rapidly. ⁸³ Subsequently, nucleation and growth process will
326 be shorten by accelerating nucleation and growth rate due to thermodynamic control of inorganic NPs.
327 Eventually, inorganic NPs with pseudo-spherical morphology or spherical one are the preferential
328 products.^{65, 84} Thus, it is reasonable to control nucleation and growth process at proper temperature to
329 modulate nucleation and growth processes under kinetic controlling for the formation of anisotropic
330 inorganic NPs. Additionally, temperature also affects growth kinetics of inorganic NPs by shifting the
331 established equilibrium between inorganic NPs and participated species in solution state through

332 varying the activity of stabilizers or additives and the chemical state of inorganic NPs. Hence, varying
333 temperature for nucleation and growth process can be prevalent route for control over shape of
334 inorganic NPs in solution state. For instance, as observed by Zhu and co-workers, Au plates with
335 unique and well-defined morphology has been synthesized by alternative temperature in the presence
336 of surfactants PVP through a modifying polyol process. When altering formation and precipitation
337 temperature of Au NPs, the morphology of final shape were evolved from regular of hexagonal,
338 triangle and truncated triangular plates to novel star-like and sniped shield-like Au plates, as shown in
339 **Figure 8**.⁸⁵ Additionally, controlled heating rate to aimed reaction temperature is also another route
340 for controlling nucleation and growth rate.⁸⁶

341 Generally, proper reaction temperature is a critical role to yield anisotropic shape by managing the
342 reaction procedure under kinetics control. However, it should be noted that temperature high and low
343 is relative concept, such as for the polyol method, the temperature should be varying over 120 °C.⁸⁷⁻⁸⁸
344 Under high temperature condition, aggregation,⁸⁹⁻⁹⁰ Orientated attachment,⁹¹ component diffusion
345 (such as metal alloy) and phase transition⁵⁴ are common phenomena occurring among the existed
346 particles due to minimizing free energy of the reaction system and NPs.

347 *2.3.3 Seeds and templates*

348 Seeds or templates sever as common and effective mediate for shape control of inorganic NPs.
349 Because its existed surface provides sites for further growth by depleting precursor monomer in bulk
350 solution. Here, it is worth noting that the component of seeds or templates can be as same or different
351 as the final particles, eventually generating final NPs with homogenous structure or heterogeneous
352 structure.⁴ The effective facilitated route of seeds or templates for controllable shape of inorganic NPs
353 refers as seed-mediated or template method. Seed-mediated or template growth procedure offers
354 advantage for shape control of inorganic NPs, in which the activation energy barrier for addition of
355 precursor monomers onto preformed seeds or templates is much lower, comparing with the formation
356 of new nuclei from homogenous bulk solution.⁹²⁻⁹³ However, the shape of final inorganic NPs varied
357 by seed-mediated and template route has differences that various shape of inorganic NPs can be

358 obtained by seed-mediated method, but the final shape of inorganic NPs generated by template
359 method is highly dependent on initial shape of template.

360 The size of seeds should be extremely small when seed-mediated method is carried out. Because the
361 final shape of inorganic NPs is barely affected the already formed shape of seeds if the size of initial
362 seed crystals is over the critical size.⁹⁴ Furthermore, seed amount, concentration of precursor
363 monomers, surfactants, temperatures, pH,^{13,95} etc. are significant factors for final shape of inorganic
364 NPs.⁸⁴ Particularly, in the presence of surfactants generally including CTAB/ CTAC, PVP, SDS, etc.
365 is also necessary factor for generating anisotropy shape of inorganic NPs through such seed-mediated
366 process.⁹⁶⁻⁹⁸ For instance, Liz-Marzán and co-workers have synthesized Au@Ag NPs with diverse
367 well-defined morphologies and crystalline structures through kinetic control of slow reduction and
368 stabilization of (100) facets, when employing benzyldimethylhexadecylammonium chloride as
369 stabilizer in seed-mediated method. The adsorption of halide ions Cl⁻ from stabilizer caused
370 significantly change of surface energies of different facets, as confirmed by density functional theory
371 calculations of surface energies. Eventually, single crystalline core-shell Au@Ag cubes enclosed by
372 six (100) facets were evolved from initial single crystalline Au core with octahedra and nanorods
373 shape due to the adsorption of Cl⁻ on (100) facet, while core-shell Au@Ag nanorods with an increased
374 aspect ratio were produced from the originated pentatwinned Au nanorods by adsorbing of AgCl on
375 (100) and (110) facets.⁹⁹

376 Additionally, seed-mediated method also is easily achieved for inorganic NPs with high-index facets,
377 ⁶² core-shell structure, branch or alloy.⁶³ For instance, colloidal wurtzite crystal structures (wz-CdSe)
378 including nanocubes, hexagonal nanoplatelets, nanorod and bullet-shaped particles were yielded
379 through seed-mediated method by using small (2-3 nm) wz-CdSe nanocrystals as seed, as shown in
380 **Figure 9**. Selective growth of different facets on seed nanocrystals driven the initial shape of wz-
381 CdSe to differential one. Radial growth from the (002) face at high concentration of precursor and
382 higher reaction temperature 370 °C lead to wz-CdSe hexagonal platelets, while preferentially adding
383 precursor monomers onto (002) and (00-2) facets of seeds at low precursor concentration and lower

384 reaction temperature 350 °C formed wz-CdSe nanorods.¹⁰⁰ Additionally, multi-step seed mediated
385 technique also can be applied for controlling over shape of inorganic NPs. ¹⁰¹⁻¹⁰² However,
386 concentration of seed and precursors, reaction temperature, pH and growth time are also significant
387 parameters to control anisotropic shape of inorganic NPs during seed-mediated process.¹⁰³

388 *2.3.4 Surfactants or additives*

389 Most of inorganic NPs have strong tendency to aggregate into bigger particles with irregular and
390 undesirable morphologies during growth procedure in bulk solution due to their high surface free
391 energy of nanoscale size. To address this shortcoming, surfactants and additives are considered as
392 excellent candidates of shape modulator in bulk solution, with expect that surfactants or additives can
393 adsorb onto some facets of growing NPs dynamically to reduce their surface energy and render
394 controllable growth rate of specific facets for desirable morphology of inorganic NPs. Furthermore,
395 stabilized layers formed by surfactants or additives on the surface of NPs also protect particles against
396 aggregation in solution state. ¹⁰⁴⁻¹⁰⁵ Generally, surfactants or additives are composed of functional or
397 coordinating groups, which is the key role as capping agent to adsorb onto the surface of growing NPs.
398 Thus, the adsorption ability and stability of functional or coordinating groups should be well
399 considered for selection of capping agents. As such, the capping agents commonly used for synthesis
400 of inorganic NPs with tunable shape are small molecules and polymers. The functional or
401 coordinating groups from small molecules and polymers such as hydroxyl group, ¹⁰⁶ amine groups
402 (primary, secondary and tertiary amine group), ¹⁰⁷⁻¹⁰⁸ thiol groups, and a long alkyl chain are
403 considered as selective adsorbed groups onto special facets of NPs. Common polymers are poly-
404 (vinylpyrrolidone) (PVP), ¹⁰⁹⁻¹¹¹ poly(acrylic acid) (PAA) and poly (allylamine hydrochloride) (PAH)
405 ¹¹² polyetherimide (PEI),¹¹³ poly(vinyl alcohol) (PVA),¹¹⁴ poly(ethylene glycol) (PEG) and complexes
406 of PEGylated polymers.¹¹⁵⁻¹¹⁶ Typical small molecules are including cetyltrimethylammonium
407 bromide (CTAB), ¹¹⁷⁻¹¹⁸ cetyltrimethylammonium chloride (CTAC),⁶² oleic acid and/or oleylamine,^{53,}
408 ¹¹⁹ trioctylphosphine oxide (TOPO),⁴ octadecylamine (ODA),⁸⁷ and trioctylphosphine (TOP),¹¹⁶
409 sodium dodecyl sulfate (SDS). ¹²⁰ Additionally, strong interaction between halides (Cl⁻, Br⁻, I⁻) from
410 small molecules and surface of NPs is another common controlled role for modulating shape of NPs

411 by selective growth, particularly for novel metals.^{45, 98-99, 121-122} Adsorption of functional or
412 coordinating groups onto different crystal planes of NPs is not limited within small molecules and
413 long-chain polymers,¹²³⁻¹²⁴ some solvents with functional or coordinating groups also provide similar
414 adsorption ability as the small molecules and polymers,¹¹¹ such as, N, N-dimethylformamide
415 (DMF),^{37, 125} EG.¹²⁶ Here, the relationships of small molecules, polymers and solvents for shape
416 modulation of NPs and typical shape of different materials by adsorption of functional or coordinating
417 groups are clearly summarized in **Figure 10**.^{119, 127-137}

418 Besides single surfactant and additive employing as capping agent, a mixture of different surfactants
419 together also provides capping ability in controlling nucleation and growth process of NPs due to their
420 synergistic interaction of multiple functional or coordinating groups with metal ions and different
421 facets of NPs.¹³⁸⁻¹³⁹ Binary surfactants of PVP and metal-halides salts (MCl_x , $x=1, 2, 3$, such as $FeCl_3$,
422 $CuCl_2$, $NaCl$) were added to synthesize 2D Au nanosheets with triangular and hexagonal morphology
423 in polyol process. Although, PVP adsorbed on (111) facet for producing of Au nanosheet, a mixed
424 suspension with nanosheets and spherical particles still was obtained at high concentration of PVP.
425 With the adsorption assistance of metal-halides salts, mass of solely nanosheets was yielded.¹²⁷

426 Additionally, surfactants are considered as soft templates in emulsion process or some typical
427 reactions.^{105, 140} In the emulsion synthesis process, fluxional structures droplets including vesicles,
428 micelles and reverse micelles were postulated to behave as soft reactors or templates. Normally, these
429 soft templates are composed of diverse molecules including block copolymers, liquid crystals, and
430 large biological molecules such as fatty acids.^{115, 141} Applying PVP, CTAB and SDS as soft templates,
431 cobalt nanowires, nanocubes and hollow spheres can be synthesized. As proposed by Yuhua Shen and
432 co-workers, by using Gemini surfactants (double sodium-sulfonic polyethylene glycol laurate (C_{12} -
433 PEG- C_{12})) as soft template, polyhedrons $BaCrO_4$ and rod-like $PbCrO_4$ micro/nanocrystals was
434 prepared. The size and morphology of $BaCrO_4$ and $PbCrO_4$ micro/nanocrystals were controlled by
435 altering the spacer length of soft template C_{12} -PEG- C_{12} , indicating that the lengths of polyethylene
436 glycol group spacers in Gemini surfactants had different interfacial adsorption on particles surface
437 determining size and shape of $MCrO_4$ micro/nanoparticles.¹¹⁵

438 **3 The shape-controlled mechanisms**

439 In the past three decades, a great of efforts have been devoted to control various inorganic NPs with
440 tunable shape, and several different mechanisms also have been explored through their nucleation and
441 growth process at crystallographic level, such as, selective adsorption and growth, underpotential
442 deposition, Orientation attachment, self-assembly, etc. Here, basic principle of each mechanism for
443 shape controlling of inorganic NPs is illustrated, subsequently general shapes of inorganic NPs
444 obtained by different mechanism also are described. Meanwhile, the similarity and difference of some
445 mechanisms also have been expounded.

446 **3.1 Adsorption growth and underpotential deposition**

447 According to the Wulff's rule, surface free energy is determined by surface energy and surface area.
448 Minimizing of these surface free energies for a certain volume results in the formation of anisotropic
449 shape of NPs. Furthermore, based on Wulff construction model, growth rate of NPs is highly
450 depended on surface free energy and surface kinks of NPs.¹⁴² That is, the surface of particles with
451 higher surface free energy or surface with more number of kinks grow faster to reduce surface area
452 until achieving equilibrium of NPs surface. But, the eventual morphology of NPs is decided by the
453 slowest growth rate of crystals surface. The sufficient energy supplying to the bulk reaction solution
454 drives the generated nuclei growing fast under thermodynamic control, leading to the formation of
455 spherical NPs rather than anisotropic ones. To overcome this shortcoming, selective binding or
456 growth onto specific facets of NPs by adding surfactants or additives are the prevalent and effective
457 strategy to reduce the surface tension and alter surface properties for desirable shape of inorganic NPs.
458 A acceptable theory of selective bonding between surfactants and surface of NPs is that a particle
459 facet may with different properties (ionic facet with charges, coordinative bond, electively neutral but
460 dipolar, or highly polarizable as well as hydrophobic facet) forms electronic charge, which adsorb or
461 coordinate with opposite charge from surfactants or additives. However, the adsorption or
462 coordination of surfactant or additive onto specific facet of NPs is highly depending on concentration
463 and nature of surfactants or additives.^{130, 143}

464 As above mentioned in surfactants and additives part, diverse smaller molecules, polymers and
465 solvents with functional groups are available to adsorb selectively onto specific facets for modulating
466 shape of inorganic NPs, as shown in **Figure 10**. According to this figure, not only novel anisotropic
467 NPs with single component but also core-shell or other complex architectural NPs with multiple
468 components are enable to yield from selective growth by adding of different surfactants and additives
469 or altering concentration of surfactants and additives. For instance, core-shell Au@Ag nanocrystals
470 with different morphologies were synthesized by adding iodide ions into growth solutions consisting
471 of ascorbic acid, NaOH, and CTAB and of gold hexagonal nanoplates core. A remarkable
472 morphology of core-shell Au@Ag nanocrystals evolution was observed when adding capping agent
473 with I⁻ into the growth solution. That is, originated Au hexagonal nanoplates core was transformed to
474 hexagonal bipyramidal core-shell Au@Ag nanocrystals with increasing I⁻ amount. While unnoticeable
475 changes in morphology of core-shell Au@Ag hexagonal nanoplates were observed without adding I⁻
476 in growth solution. The reasonable explanation for this morphology evolution is that addition of I⁻ ion
477 was of benefit to the selective deposition and growth of Ag onto surface of Au hexagonal nanoplates
478 core with decreasing in surface redox potential of nanocrystals.¹²¹

479 Additionally, another phenomena underpotential deposition (UPD) causing by depositing metal cation
480 at various types of substrates (such as surface of metal or metal oxide particles) with potentials ranges
481 is more positive on shape modulation of inorganic NPs during growth process of NPs. Occurrence of
482 UPD is significantly depending on enhanced interaction between depositing metals and foreign
483 substrates during growth process due to their potential shift. Potential difference between monolayer
484 and bulk deposition causes a partial charge of adatoms.¹⁴⁴⁻¹⁴⁵ Then, chemical bond arising from this
485 partial electron transfer takes advantage for favorable deposition of the first monolayer.¹⁴⁶ Altering
486 deposited metal cations with different amount and type during UPD process promotes preferential
487 growth in a directional axis and facets to form diverse anisotropic NPs, even with high-index facets.
488 ¹⁴⁷⁻¹⁴⁹ Such as, Au NPs with different shape were produced when applying two foreign metal ions
489 Pd(II) and Ag(I) to deposit on the surface of polyhedral gold nanocrystals in one-pot polyol synthesis.
490 The initial Au nanocrystals were tailored to other anisotropic shapes including truncated

491 tetrahedra bounded by (310) and (111) facets, truncated ditetragonal prisms enclosed by 12
492 (310) facets, and multiple-twinned bipyramids by varying concentration ratio of Ag(I) and Pd(II) in a
493 growth solution (**Figure 11**). It was noted that the morphology of Au nanocrystals were different
494 when Ag(I) and Pd(II) were introduced separately. That is, tetrahedra Au bounded with (110)
495 facets was formed only with Ag UPD, while Au truncated octahedra and triangular plates with (100)
496 facets were facilitated with only Pd deposition.¹² Additionally, as investigated by Mirkin group, Ag
497 ions was served as an UPD agent to access a different set of Au NPs with adjustable shapes by
498 controlling growth of the existed Au NPs through surface passivation (more so than kinetic effects).
499 Decreasing stability of the underpotentially deposited Ag layer in the presence of larger halides
500 contributes to the shape evolution due to the relative strengths of the Ag^+/Ag^0 -halide and
501 Au^+/Au^0 -halide interactions.¹⁵⁰

502 **3.2 Agglomeration and aggregation**

503 Aggregation is a common and complex phenomenon for collision of NPs, causing difficulty in
504 exploring their properties and applications of nanostructured materials. A common and reasonable
505 explanation for aggregation among NPs is high surface free energy of their tiny nanoscale size. Two
506 key parameters are required for occurrence of aggregation including a Brownian or flow motion that
507 brings particles into proximity of each other, and a net interparticle attractive force. Thus, a direct
508 mutual attraction among particles (such as van der Waals forces or chemical bonding), is bonded for
509 aggregated NPs through such motion and attraction.¹⁵¹ Usually, aggregation takes place in the
510 reaction solution with high concentration of small NPs, high temperature and slow agitation speed.
511 However, aggregation always being avoided during the colloid science process due to uncontrollable
512 morphology, undesirable properties and unsatisfied applications in the past decades.¹⁵² To avoid
513 aggregation, coating with foreign capping agents and/or changing the surface charges of performed
514 NPs is the effective and tailored route.^{151, 153-154} Recently, with assistance of foreign capping agents or
515 surfactants, various anisotropic shape of inorganic NPs, such as wires,¹⁵⁵ polyhedron,⁵⁰ coral-like,¹⁵²
516 etc.^{38, 90, 156-158} can be obtained by controllable aggregation. For instance, Pt NPs with a variety of
517 morphologies including cubes, octahedrons, cuboctahedrons and tetrahedrons by adding of silver

518 nitrate and stabilizer of PVP have been prepared through a modified polyol method. The altered
519 shapes of Pt NPs from cube to multiple-branched nanostructures were highly related with the amount
520 of silver nitrate, reaction time and temperature during the aggregation process of initial nuclei. With
521 overgrowth and aggregation of initial Pt nuclei instantly, multiple-branched Pt nanostructures were
522 formed at higher amount of AgNO_3 0.06 M within reaction time 30 min. Whereas, due to aggregation
523 of Pt clusters or initial Pt seeds, even small Pt nanocrystals, cubic and octahedral Pt NPs were formed
524 in presence of lower amount of AgNO_3 0.04 M within 5-15 min.¹⁵⁹

525 According to Macy and Cournil's report, collision and physical adhesion cause the aggregation among
526 particles, and the binding force between individual NPs in aggregation is rather weak. However, the
527 aggregated NPs becoming a concrete body with addition of molecules onto surface and continuous
528 growth refer as agglomeration.¹⁶⁰ It should be noticed that agglomeration is different mechanism from
529 aggregation. However, those two concepts have been mixed up in many literatures. Here, clear
530 definition and difference are conducted, as elaborated in **Figure 12**. Aggregation of particles is formed
531 through classical nucleation, growth, collision and attachment, thus, aggregated particles form among
532 the generated concrete NPs. While, the route to form agglomerated particles is through clusters
533 aggregation, nucleation and growth. Then, the agglomerated particles generates from atomic cluster of
534 different components, but eventually formed particles with uniformed components, such as spinel
535 ferrites (MFe_2O_4 (M =Mn, Fe, Co, Ni)),¹⁶¹⁻⁵⁰ metal carbonate (MCO_3 or MSO_4 , M=Ca, Mg, Sr).¹⁶²⁻¹⁶³
536 For instance, as reported by Gupta and co-workers, they used thermolysis of $\text{Co}^{2+}\text{Fe}_2^{3+}$ oleate complex
537 in organic solution to obtain monodisperse magnetic cobalt ferrite (CoFe_2O_4) nanocrystals by
538 agglomeration mechanism. During this process, the growth dynamics of particles dictated shape
539 controlling process of CoFe_2O_4 nanocrystals. Furthermore, the reproducible CoFe_2O_4 nanocrystals
540 evolving from initial spherical, to spherical-to-cubic, cubic, corner-grown cubic, or starlike shapes
541 were controlled by prolonging aging time.⁸⁶

542 Additionally, the force among particles in aggregation and agglomeration is different that the direct
543 force among particles causing by aggregation is van der Waals force, but the force exists in

544 agglomerated particles is chemical bonding such as hydrogen bonding, which is much higher than the
545 force in aggregated particles. The final shape of inorganic NPs resulted by aggregation and
546 agglomeration is different that the shape causing by aggregation is undefined one, whereas the shape
547 causing by agglomeration usually is spherical one.¹⁶⁴⁻¹⁶⁶ Furthermore, the general size of particles
548 generated by agglomeration is micro-scale.¹⁶⁷⁻¹⁶⁸

549 **3.3 Orientation attachment and self-assembly**

550 In 1998, Penn and Banfield discovered an important crystal growth mechanism named “oriented
551 attachment” (OA),¹⁶⁹ involving spontaneous self-organization of adjacent particles and continuous
552 growth of the self-organized particles at initial step. Then, the self-organized particles share a common
553 crystallographic orientation and join at a planar interface.¹⁷⁰ During this process, fusion among the
554 previous formed NPs is driving force for sharing a common crystallographic orientation. However,
555 this fusion caused crystallographic orientation also can affect by other factors in the reaction solution,
556 resulting in different pathways yielding of iso-oriented hybrid crystals, mesocrystals, and single
557 crystals.¹⁷¹

558 The acceptable explanation for occurrence of OA is that particles attach with each other at their high-
559 energy facets to eliminate surface energy. After such attachment, eliminating these high-energy facets
560 and fusing in crystallographically form a secondary complete anisotropic particle. During this process
561 of OA, the intermediate steps may relate with effect collision or agglomeration and realignment
562 processes. Current researches have been suggested that OA may occur by collisions of aligned
563 nanocrystals in suspension or rotation of misaligned NPs in contacting toward low-energy interface
564 configurations.¹⁷² Thus, a successive collisions or direct contact is the key factor for formation of
565 anisotropic particles by OA during dispersed or agglomerated conditions. Until recently, this
566 speculation of OA process has been demonstrated through direct observation of iron oxyhydroxide
567 NPs under high-resolution transmission electron microscopy (HRTEM) using a fluid cell (as shown in
568 **Figure 13**). According to their observation, particles undergo continuous rotation and interaction to
569 each other until some particles find a perfect lattice match. Within a distance less than 1 nanometer, a

570 sudden jump of one particle to another one and contact together, lateral atom-by-atom addition initiate
571 at the contact point of attached particles subsequently, as observed in **Figure 10 (f)** to **Figure 10 (g)**.
572 This interface elimination proceeds at a rate consistent with the curvature dependence of Gibbs free
573 energy. Based on measured translational and rotational accelerations, strong and highly direction-
574 specific interaction is the direct driving force for particles growth via OA.¹⁷³ Additionally, OA also has
575 been found to be a significant mechanism in controlling growth to obtain various anisotropic
576 nanostructures, including 3D complex-shaped nanostructures by “building blocks” (architecture
577 structure), core-shell.¹⁷⁴⁻¹⁷⁶

578 Self-assembly is another common route throughout nature and technology to reconfigure shape of
579 inorganic NPs, in which autonomous organization of components into patterns or structures take place
580 without factitious intervention. The self-assembly approach includes static and dynamic self-assembly.
581 ¹⁷⁷ Here, the discussed self-assembly is static self-assembly, which is common and general occurrence
582 in atomic, ionic, and molecular or colloidal crystals system with a global or local equilibrium but
583 without energy dissipation as described by Whitesides and Grzybowski.¹⁷⁷ During this process, non-
584 covalent or weak covalent interactions (electrostatic, van der Waals, hydrophobic interactions,
585 hydrogen and coordination bonds) are the significant impacts on formation of self-assembly. Thus,
586 various surfactants and ligands are facilitated to reconfigure different ordered structure during self-
587 assembly process.¹⁷⁸⁻¹⁸³ Sun and co-workers have been synthesized successfully Pd nanowire
588 networks with lengths of a few tens of nanometers with addition of sodium citrate though an inherent
589 self-assembly process, in which strong electrostatic absorption between Pd NPs and citrate groups
590 were formed.¹⁸⁴ Additionally, coating layer also induces self-assembly among performed particles to
591 reconfigure anisotropic shape of NPs. Kooij and co-workers have demonstrated that a novel 3D core-
592 shell nanoring superstructures consisting of non-dipolar Au nanorods core and magnetic Ni shells
593 have been synthesized successfully by self-assembly. Initially, magnetic dipole was induced by
594 selective reduction of Ni onto Au nanorods as coating layer, then ring-assembly to solid Ni rings with
595 Au nanorods core were closed in flux for 3D core-shell nanoring.¹⁸⁵

596 However, self-assembly of inorganic NPs on 2D substrate is largely determined by multiple factors
597 including monodispersity, shape and surface-adsorption feature of performed NPs, type of substrate
598 and reaction conditions (concentration of NPs, ambient temperature and humidity, etc.).¹⁸⁶⁻¹⁸⁸
599 Although, it is worth noting that there is difference between OA and self-assembly for shape control
600 of inorganic NPs that self-assembly is controllable process by managing the ligands or bonds among
601 particles, rather than the uncontrollable process of OA which is highly depending on the reaction
602 process and conditions.

603 **3.4 Ostwald ripening**

604 Ostwald ripening process, also known as coarsening, is a common mechanism for growth of various
605 nanomaterials, which is first proposed by Ostwald in 1900.¹⁸⁹ This mechanism is driven by chemical
606 potential of NPs increases on basis of a process of particles dissolution and ion re-precipitation,
607 resulting in increase of particles size but decrease of particles number. As described by the Gibbs-
608 Thomson relation, the local equilibrium state of solute concentration at surface of larger particles is
609 lower than that of smaller ones, resulting in solute ions flow from surface of small particles to larger
610 ones due to concentration gradient. That is, larger particles grow up at expense of smaller particles
611 until the equilibrium state of bulk solution as shown in **Figure 14**.¹⁹⁰ This growth process is often
612 under diffusion-controlled, but usually produce NPs with spherical or pseudo-spherical morphologies,
613 which are considered as more thermodynamically stable morphology.⁴² The classical kinetic model for
614 the Ostwald ripening mechanism is known as Lifshitz-Slyozov-Wagner model, basing on the Gibbs-
615 Thomson equation.

$$616 \quad \bar{D}^n - \bar{D}_0^n = k(t - t_0) \quad (11)$$

617 where \bar{D} and \bar{D}_0 are the mean size of particles at time t and t_0 , respectively. k is with respect to a
618 temperature-dependent materials constant, and n is an exponent relevant to Ostwald ripening.
619 Apparently, Ostwald ripening is time-dependent process,¹⁹¹ as direct observed 3D star Au
620 nanocrystals under the real time transmission electron microscopy (TEM) in situ two-photo scattering

621 process. The results showed that the Ostwald ripening and ripening process took place during a
622 successive formation process of nanoflower and star Au NPs, respectively. In addition, during this
623 process, the number density of initial Au nanoseeds and nanoflowers continuously decrease with time
624 for favoring another shape formation, as referenced of Ostwald ripening.¹⁹²

625 Ostwald ripening has been used widely to describe and explain particle growth with a relatively large
626 size in solution.¹²⁴ Additionally, Ostwald ripening process involves dissolution of smaller particles and
627 growth of bigger particles, which can be used to reconfigure complex shape.^{50, 193} Furthermore,
628 Ostwald ripening also can be used to explain the formation of various inorganic NPs with hollow/
629 mesoporous structure.^{50, 104, 194-195} Lou and co-workers have synthesized uniform SnO₂ hollow
630 nanospheres with large void space through a modified facile method. The void space can be varied
631 easily by reaction time, as shown in **Figure 15**. The formation of interior void space is based on an
632 inside-out Ostwald ripening mechanism, because internal unstable crystals will dissolve firstly and
633 transform to external forming a stable structure by multiple mesoporous at an early stage. More
634 importantly, this facile one-pot process with Ostwald ripening also was extended to fabricate 3D
635 rattle-type hollow structures as using α -Fe₂O₃@SnO₂ as an example, as shown in **Figure 15. (b)**.¹⁹⁶

636 **4 The prospects and outlook**

637 Significant efforts have been devoted to synthesizing of a larger number of inorganic nanomaterials
638 with uniform and tunable shape. The controlled shape of inorganic NPs could not only determine their
639 intrinsic physicochemical properties, but also offer new nanotechnologies applications in biomedicine,
640 catalysis, electronics, optical, etc. This review provides a brief account of classical theory of
641 nucleation and growth and affected factors, and general plausible mechanisms for shape control of
642 inorganic NPs toward the classical nucleation and growth theory has been described. Initially,
643 essential concepts of classical crystallization theory and general factors of nucleation and growth on
644 shape control were described to elaborate on the description of shape evolution, providing basic and
645 clear knowledge to help readers clearly figure out the correlations of experiments results with
646 synthetic conditions.^{156, 197} Despite, the general effect parameters are listed, reaction process is

647 complicate and easily affected by various factors, resulting diversity and unknown factors in shape
648 control of inorganic NPs. Thus, the reaction process and parameters should be well controlled.
649 Additionally, shape evolution of inorganic NPs from one experiment process may not be controlled by
650 one growth mechanism because of the complex reaction process. Such as, the orientated attachment
651 together with Ostwald ripening were used to explain the final shape of α -Fe₂O₃ NPs.⁵⁰

652 The process of nucleation and growth of crystals is an area of interest and well developed filed during
653 the cooling and antisolvent crystallization process, which can be confirmed by simulation process
654 according to population balance equation.¹⁹⁸⁻¹⁹⁹ However, the reacted crystallization process for shape
655 control of inorganic NPs is still far beyond predicted control because the prediction can not be made
656 as small changes within reaction conditions causing unforeseen changes within reaction mixture. Thus,
657 the shape control of inorganic NPs is still limited within empirical stage. Recently, the in situ HRTEM
658 provides a direct observation for shape evolution of particles, further analysis of these mechanisms
659 will develop the possibility to predict shape evolvement and control within solution state. Therefore,
660 obtaining controllable shape of inorganic NPs from such strategies is much faster and effective than
661 current methods of trial and error synthesis. Furthermore, the further within this shape control field of
662 inorganic NPs is relative simple and accurate as the analytical technique improving and well
663 understanding the formation mechanisms of particles on basis of nucleation and growth.

664

665 **Acknowledgment**

666 This work was supported by the NSFC (51201115, 51171132, 11375134), China Postdoctoral Science
667 Foundation (2014M550406), Hong Kong Scholars Program, Hubei Provincial Natural Science
668 Foundation (2014CFB261), the Fundamental Research Funds for the Central Universities (No.
669 2042015kf0184) and Wuhan University.

670

671 **Author Biography**



672 **Z. H. Wu**

673 **Zhaohui Wu** received her B. Sc (2007) and M. Sc on Biomedical Engineering (2011) from Hunan University of
674 Technology (Hunan, China). Her major topic was morphology and structure control of magnetic nanoparticles
675 and biology application of functional magnetic nanoparticles during the M. Sc. She is a PhD student in
676 Chemical Engineering, Kyung Hee University, Korea. She is currently researching on the crystallization process
677 controlling and product quality design including morphology, size and purity of organic crystals or inorganic
678 nanoparticles. Her multidisciplinary research involves inorganic/organic materials design through crystallization
679 process and application of nanomaterials in biomedicine and functional devices.



680 **S. L. Yang**

681 **Shuanglei Yang** received his B.S. in 2007 and M.S. in 2010 from Hunan University of Technology, and he
682 received his PhD degree in 2015 under the supervision of Prof. Zhang Hongbo in Central South University. He
683 then joined the group of Prof. Yang Dongjiang at the College of Chemical and Environmental Engineering,
684 Qingdao University, as a postdoctoral fellow for the design and synthesis nanomaterials for energy conversion
685 applications. His research is focus on the synthesis, properties, and application of functional nanomaterials.

686

**W. Wu**

687

688 **Wei Wu** received his PhD degree in 2011 under the supervision of Prof. Changzhong Jiang in Department
689 of Physics, Wuhan University, China. He then joined the group of Prof. Daiwen Pang at Wuhan University
690 (2011) and Prof. V. A. L. Roy at City University of Hong Kong (2014) as a postdoctoral fellow. Now he is
691 the Director and Associate Professor of the Laboratory of Printable Functional Nanomaterials and Printed
692 Electronics, School of Printing and Packaging, Wuhan University. He has published, as an author and co-
693 author, more than 70 publications in various reputed international journals and his papers have been cited
694 more than 1200 times.. He is also an Associate Editor of *Journal of Nanoscience Letters*, and editorial
695 board member of *Advanced Science, Engineering and Medicine* and *Journal of Green Science and*
696 *Technology*, his research interests include the synthesis and application of functional nanomaterials,
697 printed electronics and sensors.

698

699 **References**

- 700 1. Chiu, T. C.; Huang, C. C., Aptamer-functionalized nano-biosensors. *Sensors-Basel* **2009**, *9*
701 (12), 10356-10388.
- 702 2. Xie, J. P.; Zhang, Q. B.; Lee, J. Y.; Wang, D. I. C., The synthesis of SERS-active gold
703 nanoflower tags for in vivo applications. *ACS Nano* **2008**, *2* (12), 2473-2480.
- 704 3. Seifert, G.; Stalmashonak, A.; Hofmeister, H.; Haug, J.; Dubiel, M., Laser-induced,
705 polarization dependent shape transformation of Au/Ag nanoparticles in glass. *Nanoscale Res. Lett.*
706 **2009**, *4* (11), 1380-1383.
- 707 4. Buonsanti, R.; Grillo, V.; Carlino, E.; Giannini, C.; Gozzo, F.; Garcia-Hernandez, M.; Garcia,
708 M. A.; Cingolani, R.; Cozzoli, P. D., Architectural control of seeded-grown magnetic-semiconductor
709 iron oxide-TiO₂ nanorod heterostructures: The role of seeds in topology selection. *J. Am. Chem. Soc.*
710 **2010**, *132* (7), 2437-2464.
- 711 5. Wu, W.; Jiang, C. Z.; Roy, V. A. L., Recent progress in magnetic iron oxide–semiconductor
712 composite nanomaterials as promising photocatalysts. *Nanoscale* **2015**, *7*, 38-58.
- 713 6. Xia, K.; Zhang, L. M.; Huang, Y. F.; Lu, Z. X., Preparation of gold nanorods and their
714 applications in photothermal therapy. *J. Nanosci. Nanotechnol.* **2015**, *15* (1), 63-73.
- 715 7. Zhang, L. M.; Wang, Z. X.; Lu, Z. X.; Xia, K.; Deng, Y.; Li, S.; Zhang, C. X.; Huang, Y. F.;
716 He, N. Y., Synthesis of LiYF₄: Yb, Er upconversion nanoparticles and its fluorescence properties. *J.*
717 *Nanosci. Nanotechnol.* **2014**, *14* (6), 4710-4713.
- 718 8. Bulgarini, G.; Reimer, M. E.; Zehender, T.; Hocevar, M.; Bakkers, E. P. A. M.;
719 Kouwenhoven, L. P.; Zwiller, V., Spontaneous emission control of single quantum dots in bottom-up
720 nanowire waveguides. *Appl. Phys. Lett.* **2012**, *100* (12), 121106.
- 721 9. Bozon-Verduraz, F.; Fievet, F.; Piquemal, J. Y.; Brayner, R.; El Kabouss, K.; Soumare, Y.;
722 Viau, G.; Shafeev, G., Nanoparticles of metal and metal oxides: some peculiar synthesis methods, size
723 and shape control, application to catalysts preparation. *Braz. J. Phys.* **2009**, *39* (1A), 134-140.
- 724 10. Lizandara-Pueyo, C.; Morant-Minana, M. C.; Wessig, M.; Krumm, M.; Mecking, S.; Polarz,
725 S., Biomimetic crystallization of anisotropic zinc oxide nanoparticles in the homogeneous phase:
726 shape control by surface additives applied under thermodynamic or kinetic control. *RSC Adv.* **2012**, *2*
727 (12), 5298-5306.
- 728 11. Nguyen, T. D., From formation mechanisms to synthetic methods toward shape-controlled
729 oxide nanoparticles. *Nanoscale* **2013**, *5* (20), 9455-9482.
- 730 12. Toan, T. T.; Lu, X. M., Synergistic effect of Ag and Pd ions on shape-selective growth of
731 polyhedral Au nanocrystals with high-index facets. *J. Phys. Chem. C* **2011**, *115* (9), 3638-3645.
- 732 13. Xu, Z. C.; Shen, C. M.; Xiao, C. W.; Yang, T. Z.; Zhang, H. R.; Li, J. Q.; Li, H. L.; Gao, H. J.,
733 Wet chemical synthesis of gold nanoparticles using silver seeds: a shape control from nanorods to
734 hollow spherical nanoparticles. *Nanotechnology* **2007**, *18* (11), 115608.

- 735 14. Zhang, L. M.; Xia, K.; Lu, Z. X.; Li, G. P.; Chen, J.; Deng, Y.; Li, S.; Zhou, F. M.; He, N. Y.,
736 Efficient and facile synthesis of gold nanorods with finely tunable plasmonic peaks from visible to
737 Near-IR range. *Chem. Mater.* **2014**, *26* (5), 1794-1798.
- 738 15. Lu, Z. X.; Huang, Y. F.; Zhang, L. M.; Xia, K.; Deng, Y.; He, N. Y., Preparation of gold
739 nanorods using 1,2,4-Trihydroxybenzene as a reducing agent. *J. Nanosci. Nanotechnol.* **2015**, *15* (8),
740 6230-6235.
- 741 16. Li, X. L.; Zhang, F. Q.; Ma, C.; Deng, Y.; Wang, Z. F.; Elingarami, S.; He, N. Y.,
742 Controllable synthesis of ZnO with various morphologies by hydrothermal method. *J. Nanosci.*
743 *Nanotechnol.* **2012**, *12* (3), 2028-2036.
- 744 17. Lv, H. L.; Ji, G. B.; Liu, W.; Zhang, H. Q.; Du, Y. W., Achieving hierarchical hollow
745 carbon@Fe@Fe₃O₄ nanospheres with superior microwave absorption properties and lightweight
746 features. *J. Mater. Chem. C* **2015**, *3* (39), 10232-10241.
- 747 18. Lin, X. H.; Ji, G. B.; Liu, Y. S.; Huang, Q. H.; Yang, Z. H.; Du, Y. W., Formation mechanism
748 and magnetic properties of hollow Fe₃O₄ nanospheres synthesized without any surfactant. *Cryst. Eng.*
749 *Comm.* **2012**, *14* (24), 8658-8663.
- 750 19. Jing, H.; Zhang, Q. F.; Large, N.; Yu, C. M.; Blom, D. A.; Nordlander, P.; Wang, H., Tunable
751 plasmonic nanoparticles with catalytically active high-index facets. *Nano Lett.* **2014**, *14* (6), 3674-
752 3682.
- 753 20. Sanchez-Iglesias, A.; Grzelczak, M.; Perez-Juste, J.; Liz-Marzan, L. M., Binary Self-
754 assembly of gold nanowires with nanospheres and nanorods. *Angew. Chem. Int. Ed.* **2010**, *49* (51),
755 9985-9989.
- 756 21. Matefi-Tempfli, S.; Habouti, S.; Matefi-Tempfli, M.; Solterbeck, C. H.; Es-Souni, M.; Es-
757 Souni, M., Self-standing corrugated Ag and Au-nanorods for plasmonic applications. *J. Mater. Chem.*
758 **2011**, *21* (17), 6269-6273.
- 759 22. Rodriguez-Lorenzo, L.; Romo-Herrera, J. M.; Perez-Juste, J.; Alvarez-Puebla, R. A.; Liz-
760 Marzan, L. M., Reshaping and LSPR tuning of Au nanostars in the presence of CTAB. *J. Mater. Chem.*
761 **2011**, *21* (31), 11544-11549.
- 762 23. Zhang, H.; Huang, X.; Qi, X. Y.; Huang, Y. Z.; Li, S. Z.; Xue, C.; Gan, C. L.; Boey, F.,
763 Photochemically controlled synthesis of anisotropic Au nanostructures: Platelet-like Au nanorods and
764 six-star Au nanoparticles. *ACS Nano* **2010**, *4* (10), 6196-6202.
- 765 24. Zhang, H.; Jin, M. S.; Xiong, Y. J.; Lim, B.; Xia, Y. N., Shape-controlled synthesis of Pd
766 nanocrystals and their catalytic applications. *Acc. Chem. Res.* **2013**, *46* (8), 1783-1794.
- 767 25. Ke, F. S.; Solomon, B.; Ding, Y.; Xu, G. L.; Sun, S. G.; Wang, Z. L.; Zhou, X. D., Enhanced
768 electrocatalytic activity on gold nanocrystals enclosed by high-index facets for oxygen reduction.
769 *Nano Energy* **2014**, *7*, 179-188.
- 770 26. Ho, C. H.; Tsai, C. P.; Chung, C. C.; Tsai, C. Y.; Chen, F. R.; Lin, H. J.; Lai, C. H., Shape-

- 771 controlled growth and shape-dependent cation site occupancy of monodisperse Fe₃O₄ nanoparticles.
772 *Chem. Mater.* **2011**, *23* (7), 1753-1760.
- 773 27. Radi, A.; Pradhan, D.; Sohn, Y.; Leung, K. T., Nanoscale shape and size control of cubic,
774 cuboctahedral, and octahedral Cu-Cu₂O core-shell nanoparticles on Si(100) by one-step, templateless,
775 capping-agent-free electrodeposition. *ACS Nano* **2010**, *4* (3), 1553-1560.
- 776 28. Chang, J.; Waclawik, E. R., Colloidal semiconductor nanocrystals: controlled synthesis and
777 surface chemistry in organic media. *RSC Adv.* **2014**, *4* (45), 23505-23527.
- 778 29. Tao, A. R.; Habas, S.; Yang, P. D., Shape control of colloidal metal nanocrystals. *Small* **2008**,
779 *4* (3), 310-325.
- 780 30. Wu, W.; Wu, Z. H.; Yu, T.; Jiang, C. Z.; Kim, W. S., Recent progress on magnetic iron oxide
781 nanoparticles: synthesis, surface functional strategies and biomedical applications. *Sci. Technol. Adv.*
782 *Mat.* **2015**, *16* (2), 023501.
- 783 31. Mullin, J. W., *Crystallization*. 4th ed.; Butterworth-Heinemann: Oxford ; Boston, 2001, 594.
- 784 32. Thanh, N. T. K.; Maclean, N.; Mahiddine, S., Mechanisms of nucleation and growth of
785 nanoparticles in solution. *Chem. Rev.* **2014**, *114* (15), 7610-7630.
- 786 33. Gilroy, K. D.; Hughes, R. A.; Neretina, S., Kinetically controlled nucleation of silver on
787 surfactant-free gold seeds. *J. Am. Chem. Soc.* **2014**, *136* (43), 15337-15345.
- 788 34. Min, Y.; Kwak, J.; Soon, A.; Jeong, U., Nonstoichiometric nucleation and growth of
789 multicomponent nanocrystals in solution. *Acc. Chem. Res.* **2014**, *47* (10), 2887-2893.
- 790 35. Sun, Y. G., Controlled synthesis of colloidal silver nanoparticles in organic solutions:
791 empirical rules for nucleation engineering. *Chem. Soc. Rev.* **2013**, *42* (7), 2497-2511.
- 792 36. Wagle, D. V.; Zhao, H.; Baker, G. A., Deep eutectic solvents: Sustainable media for
793 nanoscale and functional materials. *Acc. Chem. Res.* **2014**, *47* (8), 2299-2308.
- 794 37. Sun, W.; Liu, H.; Hu, J. C.; Li, J., Controllable synthesis and morphology-dependent
795 photocatalytic performance of anatase TiO₂ nanoplates. *RSC Adv.* **2015**, *5* (1), 513-520.
- 796 38. Song, R. Q.; Colfen, H.; Xu, A. W.; Hartmann, J.; Antonietti, M., Polyelectrolyte-directed
797 nanoparticle aggregation: Systematic morphogenesis of calcium carbonate by nonclassical
798 crystallization. *ACS Nano* **2009**, *3* (7), 1966-1978.
- 799 39. Yang, Y.; Wang, H.; Ji, Z.; Han, Y. S.; Li, J. H., A switch from classic crystallization to non-
800 classic crystallization by controlling the diffusion of chemicals. *Cryst. Eng. Comm.* **2014**, *16* (33),
801 7633-7637.
- 802 40. Ackerman, D. M.; Evans, J. W., Boundary conditions for burton-cabrera-frank type step-flow
803 models: Coarse-graining of discrete 2d deposition-diffusion equations. *Multiscale Model. Sim.* **2011**, *9*
804 (1), 59-88.
- 805 41. Sugimoto, T., *Monodispersed Particles*. Elsevier B.V. : Amsterdam, 2001.
- 806 42. Zong, R. L.; Wang, X. L.; Shi, S. K.; Zhu, Y. F., Kinetically controlled seed-mediated growth

- 807 of narrow dispersed silver nanoparticles up to 120 nm: secondary nucleation, size focusing, and
808 Ostwald ripening. *Phys. Chem. Chem. Phys.* **2014**, *16* (9), 4236-4241.
- 809 43. Luo, Y. S.; Li, S. Q.; Ren, Q. F.; Liu, J. P.; Xing, L. L.; Wang, Y.; Yu, Y.; Jia, Z. J.; Li, J. L.,
810 Facile synthesis of flowerlike Cu₂O nanoarchitectures by a solution phase route. *Cryst. Growth Des.*
811 **2007**, *7* (1), 87-92.
- 812 44. Huo, Y.; Zhu, Y. G.; Xie, J.; Cao, G. S.; Zhu, T. J.; Zhao, X. B.; Zhang, S. C., Controllable
813 synthesis of hollow alpha-Fe₂O₃ nanostructures, their growth mechanism, and the morphology-
814 reserved conversion to magnetic Fe₃O₄/C nanocomposites. *RSC Adv.* **2013**, *3* (41), 19097-19103.
- 815 45. Chien, Y. H.; Tsai, M. F.; Shanmugam, V.; Sardar, K.; Huang, C. L.; Yeh, C. S., Escape from
816 the destruction of the galvanic replacement reaction for solid - hollow - solid conversion process in
817 one pot reaction. *Nanoscale* **2013**, *5* (9), 3863-3871.
- 818 46. Wang, S. C.; Ray-Kuang, C. B.; Hu, P. J., Morphological and phase control of tin oxide
819 single-crystals synthesized by dissolution and recrystallization of bulk SnO powders. *J. Eur. Ceram.*
820 *Soc.* **2011**, *31* (14), 2447-2451.
- 821 47. Zhou, X. P.; Ni, S. Y.; Zhang, X.; Wang, X. Q.; Hu, X. H.; Zhou, Y., Controlling shape and
822 size of TiO₂ nanoparticles with sodium acetate. *Curr. Nanosci.* **2008**, *4* (4), 397-401.
- 823 48. Fuji, M.; Shin, T.; Watanabe, H.; Takei, T., Shape-controlled hollow silica nanoparticles
824 synthesized by an inorganic particle template method. *Adv. Powder Technol.* **2012**, *23* (5), 562-565.
- 825 49. Obare, S. O.; Jana, N. R.; Murphy, C. J., Preparation of polystyrene- and silica-coated gold
826 nanorods and their use as templates for the synthesis of hollow nanotubes. *Nano Lett.* **2001**, *1* (11),
827 601-603.
- 828 50. Lin, M.; Tan, H. R.; Tan, J. P. Y.; Bai, S. Q., Understanding the growth mechanism of α -
829 Fe₂O₃ nanoparticles through a controlled shape transformation. *J. Phys. Chem. C* **2013**, *117* (21),
830 11242-11250.
- 831 51. Wu, W.; Xiao, X. H.; Zhang, S. F.; Zhou, J. A.; Fan, L. X.; Ren, F.; Jiang, C. Z., Large-scale
832 and controlled synthesis of iron oxide magnetic short nanotubes: Shape evolution, growth mechanism,
833 and magnetic properties. *J. Phys. Chem. C* **2010**, *114* (39), 16092-16103.
- 834 52. Do, T. O.; Nguyen, T. D.; Dinh, C. T., A general procedure to synthesize highly crystalline
835 metal oxide and mixed oxide nanocrystals in aqueous medium and photocatalytic activity of
836 metal/oxide nanohybrids. *Nanoscale* **2011**, *3* (4), 1861-1873.
- 837 53. Yong, K. T.; Sahoo, Y.; Swihart, M. T.; Prasad, P. N., Shape control of CdS nanocrystals in
838 one-pot synthesis. *J. Phys. Chem. C* **2007**, *111* (6), 2447-2458.
- 839 54. Feigl, C. A.; Barnard, A. S.; Russo, S. P., Modelling polar wurtzite ZnS nanoparticles: the
840 effect of sulphur supersaturation on size- and shape-dependent phase transformations. *J. Mater. Chem.*
841 **2012**, *22* (36), 18992-18998.
- 842 55. LaMer, V. K.; Dinegar, R. H., Theory, production and mechanism of formation of

- 843 monodispersed hydrosols. *J. Am. Chem. Soc.* **1950**, *72* (11), 4847-4854.
- 844 56. Huang, Y.; Pemberton, J. E., Synthesis of uniform, spherical sub-100 nm silica particles
845 using a conceptual modification of the classic LaMer model. *Colloid Surf. A* **2010**, *360* (1-3), 175-183.
- 846 57. Mdluli, P. S.; Sosibo, N. M.; Mashazi, P. N.; Nyokong, T.; Tshikhudo, R. T.; Skepu, A.; van
847 der Lingen, E., Selective adsorption of PVP on the surface of silver nanoparticles: A molecular
848 dynamics study. *J. Mol. Struct.* **2011**, *1004* (1-3), 131-137.
- 849 58. Lin, H. X.; Lei, Z. C.; Jiang, Z. Y.; Hou, C. P.; Liu, D. Y.; Xu, M. M.; Tian, Z. Q.; Xie, Z. X.,
850 Supersaturation-dependent surface structure evolution: From ionic, molecular to metallic
851 micro/nanocrystals. *J. Am. Chem. Soc.* **2013**, *135* (25), 9311-9314.
- 852 59. Wang, J.; Hou, S. C.; Zhang, L. Z.; Chen, J. C.; Xiang, L., Ultra-rapid formation of ZnO
853 hierarchical structures from dilution-induced supersaturated solutions. *Cryst. Eng. Comm.* **2014**, *16*
854 (30), 7115-7123.
- 855 60. Wang, X. G., Ammonium mediated hydrothermal synthesis of nanostructured hematite (α -
856 Fe_2O_3) particles. *Mater. Res. Bull.* **2012**, *47* (9), 2513-2517.
- 857 61. Liakakos, N.; Cormary, B.; Li, X. J.; Lecante, P.; Respaud, M.; Maron, L.; Falqui, A.;
858 Genovese, A.; Vendier, L.; Koinis, S.; Chaudret, B.; Soulantica, K., The big impact of a small detail:
859 Cobalt nanocrystal polymorphism as a result of precursor addition rate during stock solution
860 preparation. *J. Am. Chem. Soc.* **2012**, *134* (43), 17922-17931.
- 861 62. Lee, J. Y.; Yu, Y.; Zhang, Q. B.; Lu, X. M., Seed-mediated synthesis of monodisperse
862 concave trisoctahedral gold nanocrystals with controllable sizes. *J. Phys. Chem. C* **2010**, *114* (25),
863 11119-11126.
- 864 63. DeSantis, C. J.; Weiner, R. G.; Radmilovic, A.; Bower, M. M.; Skrabalak, S. E., Seeding
865 bimetallic nanostructures as a new class of plasmonic colloids. *J. Phys. Chem. Lett.* **2013**, *4* (18),
866 3072-3082.
- 867 64. Eguchi, M.; Mitsui, D.; Wu, H. L.; Sato, R.; Teranishi, T., Simple reductant concentration-
868 dependent shape control of polyhedral gold nanoparticles and their plasmonic properties. *Langmuir*
869 **2012**, *28* (24), 9021-9026.
- 870 65. Wan, Y.; Guo, Z. R.; Jiang, X. L.; Fang, K.; Lu, X.; Zhang, Y.; Gu, N., Quasi-spherical silver
871 nanoparticles: Aqueous synthesis and size control by the seed-mediated Lee-Meisel method. *J.*
872 *Colloid Interf. Sci.* **2013**, *394*, 263-268.
- 873 66. Sugimoto, T.; Zhou, X. P.; Muramatsu, A., Synthesis of uniform anatase TiO_2 nanoparticles
874 by gel-sol method: 3. Formation process and size control. *J. Colloid Interf. Sci.* **2003**, *259* (1), 43-52.
- 875 67. Harn, Y. W.; Yang, T. H.; Tang, T. Y.; Chen, M. C.; Wu, J. M., Facet-dependent
876 photocatalytic activity and facet-selective etching of silver(I) oxide crystals with controlled
877 morphology. *Chem. Cat. Chem.* **2015**, *7* (1), 80-86.
- 878 68. Bell, S. E. J.; Papadopoulou, E., Structure of adenine on metal nanoparticles: pH equilibria

- 879 and formation of Ag⁺ complexes detected by surface-enhanced Raman spectroscopy. *J. Phys. Chem. C*
880 **2010**, *114* (51), 22644-22651.
- 881 69. Rao, X. H.; Su, X. T.; Yang, C.; Wang, J. D.; Zhen, X. P.; Ling, D., From spindle-like β-
882 FeOOH nanoparticles to α-Fe₂O₃ polyhedral crystals: shape evolution, growth mechanism and gas
883 sensing property. *Cryst. Eng. Comm.* **2013**, *15* (36), 7250-7256.
- 884 70. Xu, L.; Yang, X. Y.; Zhai, Z.; Chao, X.; Zhang, Z. H.; Hou, W. H., EDTA-mediated
885 hydrothermal synthesis of NaEu(MoO₄)₂ microrugbies with tunable size and enhanced luminescence
886 properties. *Cryst. Eng. Comm.* **2011**, *13* (15), 4921-4929.
- 887 71. Okitsu, K.; Sharyo, K.; Nishimura, R., One-pot synthesis of gold nanorods by ultrasonic
888 irradiation: The effect of pH on the shape of the gold nanorods and nanoparticles. *Langmuir* **2009**, *25*
889 (14), 7786-7790.
- 890 72. Chen, K. F.; Xue, D. F., pH-assisted crystallization of Cu₂O: Chemical reactions control the
891 evolution from nanowires to polyhedra. *Cryst. Eng. Comm.* **2012**, *14* (23), 8068-8075.
- 892 73. Alqadi, M. K.; Noqtah, O. A. A.; Alzoubi, F. Y.; Alzoubi, J.; Aljarrah, K., pH effect on the
893 aggregation of silver nanoparticles synthesized by chemical reduction. *Mater. Sci-Poland* **2014**, *32* (1),
894 107-111.
- 895 74. Jia, C.; Cheng, Y.; Bao, F.; Chen, D. Q.; Wang, Y. S., pH value-dependant growth of α-Fe₂O₃
896 hierarchical nanostructures. *J. Cryst. Growth* **2006**, *294* (2), 353-357.
- 897 75. Niesz, K.; Reji, C.; Neilson, J. R.; Vargas, R. C.; Morse, D. E., Unusual evolution of ceria
898 nanocrystal morphologies promoted by a low-temperature vapor diffusion based process. *Cryst.*
899 *Growth Des.* **2010**, *10* (10), 4485-4490.
- 900 76. Niederberger, M.; Garnweitner, G.; Buha, J.; Polleux, J.; Ba, J.; Pinna, N., Nonaqueous
901 synthesis of metal oxide nanoparticles: Review and indium oxide as case study for the dependence of
902 particle morphology on precursors and solvents. *J. Sol-Gel Sci. Techn.* **2006**, *40*, 259-266.
- 903 77. Kobayashi, M.; Kato, H.; Kakihana, M., Synthesis of spindle and square bipyramid-shaped
904 anatase-type titanium dioxide crystals by a solvothermal method using ethylenediamine. *J. Ceram Soc.*
905 *Jpn.* **2012**, *120* (1407), 494-499.
- 906 78. Han, Y. C.; Liu, S. H.; Han, M.; Bao, J. C.; Dai, Z. H., Fabrication of hierarchical
907 nanostructure of silver via a surfactant-free mixed solvents route. *Cryst. Growth Des.* **2009**, *9* (9),
908 3941-3947.
- 909 79. Liu, J.; Xu, B.; Song, C.; Luo, H. D.; Zou, X.; Han, L. X.; Yu, X. B., Shape-controlled
910 synthesis of monodispersed nano-/micro-NaY(MoO₄)₂ (doped with Eu³⁺) without capping agents via a
911 hydrothermal process. *Cryst. Eng. Comm.* **2012**, *14* (8), 2936-2943.
- 912 80. Zhang, Z. J.; Chen, X. Y., Magnetic greigite (Fe₃S₄) nanomaterials: Shape-controlled
913 solvothermal synthesis and their calcination conversion into hematite (α-Fe₂O₃) nanomaterials. *J.*
914 *Alloy. Comp.* **2009**, *488* (1), 339-345.

- 915 81. Tsuji, M.; Nishio, M.; Jiang, P.; Miyamae, N.; Lim, S.; Matsumoto, K.; Ueyama, D.; Tang, X.
916 L., Role of chloride ions in the formation of Au@Ag core-shell nanocrystal structures by using a
917 microwave-polyol method. *Colloid Surf. A* **2008**, *317* (1-3), 247-255.
- 918 82. Biacchi, A. J.; Schaak, R. E., The solvent matters: Kinetic versus thermodynamic shape
919 control in the polyol synthesis of rhodium nanoparticles. *ACS Nano* **2011**, *5* (10), 8089-8099.
- 920 83. Goy-Lopez, S.; Castro, E.; Taboada, P.; Mosquera, V., Block copolymer-mediated synthesis
921 of size-tunable gold nanospheres and nanoplates. *Langmuir* **2008**, *24* (22), 13186-13196.
- 922 84. Bastus, N. G.; Comenge, J.; Puentes, V., Kinetically controlled seeded growth synthesis of
923 citrate-stabilized gold nanoparticles of up to 200 nm: Size focusing versus Ostwald ripening.
924 *Langmuir* **2011**, *27* (17), 11098-11105.
- 925 85. Zhu, J. J.; Kan, C. X.; Li, H. C.; Cao, Y. L.; Ding, X. L.; Wan, J. G., Synthesis and growth
926 mechanism of gold nanoplates with novel shapes. *J. Cryst. Growth* **2011**, *321* (1), 124-130.
- 927 86. Bao, N. Z.; Shen, L. M.; An, W.; Padhan, P.; Turner, C. H.; Gupta, A., Formation mechanism
928 and shape control of monodisperse magnetic CoFe₂O₄ nanocrystals. *Chem. Mater.* **2009**, *21* (14),
929 3458-3468.
- 930 87. Ibanez, M.; Guardia, P.; Shavel, A.; Cadavid, D.; Arbiol, J.; Morante, J. R.; Cabot, A.,
931 Growth kinetics of asymmetric Bi₂S₃ nanocrystals: Size distribution focusing in nanorods. *J. Phys.*
932 *Chem. C* **2011**, *115* (16), 7947-7955.
- 933 88. Wang, Z. Y.; Li, Q. F.; Fang, X. S.; Tian, X. K.; Zhang, L. D., Manipulation of the
934 morphology of CdSe nanostructures: The effect of Si. *Adv. Funct. Mater.* **2006**, *16* (5), 661-666.
- 935 89. Nguyen, T. D.; Dinh, C. T.; Do, T. O., A general procedure to synthesize highly crystalline
936 metal oxide and mixed oxide nanocrystals in aqueous medium and photocatalytic activity of
937 metal/oxide nanohybrids. *Nanoscale* **2011**, *3* (4), 1861-1873.
- 938 90. Hanus, L. H.; Sooklal, K.; Murphy, C. J.; Ploehn, H. J., Aggregation kinetics of dendrimer-
939 stabilized CdS nanoclusters. *Langmuir* **2000**, *16* (6), 2621-2626.
- 940 91. Ullah, M. H.; Kim, I.; Ha, C. S., One-step synthetic route for producing nanoslabs: Zn-
941 oriented polycrystalline and single-crystalline zinc oxide. *J. Mater. Sci.* **2006**, *41* (11), 3263-3269.
- 942 92. Lin, Z. J.; Chen, X. M.; Cai, Z. M.; Oyama, M.; Chen, X.; Wang, X. R., The initial
943 transformation mechanism of gold seeds on indium tin oxide surfaces. *Cryst. Growth Des.* **2008**, *8* (3),
944 863-868.
- 945 93. Fan, F. R.; Liu, D. Y.; Wu, Y. F.; Duan, S.; Xie, Z. X.; Jiang, Z. Y.; Tian, Z. Q., Epitaxial
946 growth of heterogeneous metal nanocrystals: From gold nano-octahedra to palladium and silver
947 nanocubes. *J. Am. Chem. Soc.* **2008**, *130* (22), 6949-6951.
- 948 94. Liu, J. C.; Duggan, J. N.; Morgan, J.; Roberts, C. B., Seed-mediated growth and
949 manipulation of Au nanorods via size-controlled synthesis of Au seeds. *J. Nanopart. Res.* **2012**, *14*
950 (12), 1289.

- 951 95. Chang, H. T.; Huang, C. C.; Yang, Z. S., Synthesis of dumbbell-shaped Au-Ag core-shell
952 nanorods by seed-mediated growth under alkaline conditions. *Langmuir* **2004**, *20* (15), 6089-6092.
- 953 96. Ahn, H. Y.; Lee, H. E.; Jin, K.; Nam, K. T., Extended gold nano-morphology diagram:
954 synthesis of rhombic dodecahedra using CTAB and ascorbic acid. *J. Mater. Chem. C* **2013**, *1* (41),
955 6861-6868.
- 956 97. Pietrobon, B.; Kitaev, V., Photochemical synthesis of monodisperse size-controlled silver
957 decahedral nanoparticles and their remarkable optical properties. *Chem. Mater.* **2008**, *20* (16), 5186-
958 5190.
- 959 98. Jin, R. C.; Garg, N.; Scholl, C.; Mohanty, A., The role of bromide ions in seeding growth of
960 Au nanorods. *Langmuir* **2010**, *26* (12), 10271-10276.
- 961 99. Gomez-Grana, S.; Goris, B.; Altantzis, T.; Fernandez-Lopez, C.; Carbo-Argibay, E.;
962 Guerrero-Martinez, A.; Almora-Barrios, N.; Lopez, N.; Pastoriza-Santos, I.; Perez-Juste, J.; Bals, S.;
963 Van Tendeloo, G.; Liz-Marzan, L. M., Au@Ag nanoparticles: Halides stabilize {100} facets. *J. Phys.*
964 *Chem. Lett.* **2013**, *4* (13), 2209-2216.
- 965 100. Rice, K. P.; Saunders, A. E.; Stoykovich, M. P., Seed-mediated growth of shape-controlled
966 wurtzite CdSe nanocrystals: Platelets, cubes, and rods. *J. Am. Chem. Soc.* **2013**, *135* (17), 6669-6676.
- 967 101. Sardar, R.; Funston, A. M.; Mulvaney, P.; Murray, R. W., Gold nanoparticles: Past, present,
968 and future. *Langmuir* **2009**, *25* (24), 13840-13851.
- 969 102. Zhang, Q. B.; Xie, J. P.; Liang, J.; Lee, J. Y., Synthesis of monodisperse Ag-Au alloy
970 nanoparticles with independently tunable morphology, composition, size, and surface chemistry and
971 their 3-D superlattices. *Adv. Funct. Mater.* **2009**, *19* (9), 1387-1398.
- 972 103. Wu, H. L.; Ji, X. H.; Zhao, L. L.; Yang, S.; Xie, R. G.; Yang, W. S., Shape evolution of
973 citrate capped gold nanoparticles in seeding approach. *Colloid Surf. A* **2012**, *415*, 174-179.
- 974 104. Xing, R. M.; Xu, F. L.; Liu, S. H.; Niu, J. Y., Surfactant-free fabrication of Fe₃O₄
975 nanospheres with selective shape. *Mater. Lett.* **2014**, *134*, 71-74.
- 976 105. Wang, W.; Howe, J. Y.; Li, Y. A.; Qiu, X. F.; Joy, D. C.; Paranthaman, M. P.; Doktycz, M. J.;
977 Gu, B. H., A surfactant and template-free route for synthesizing ceria nanocrystals with tunable
978 morphologies. *J. Mater. Chem.* **2010**, *20* (36), 7776-7781.
- 979 106. Zhang, Q.; Li, N.; Goebel, J.; Lu, Z. D.; Yin, Y. D., A systematic study of the synthesis of
980 silver nanoplates: Is citrate a "magic" reagent? *J. Am. Chem. Soc.* **2011**, *133* (46), 18931-18939.
- 981 107. Singh, A. K.; Talat, M.; Singh, D. P.; Srivastava, O. N., Biosynthesis of gold and silver
982 nanoparticles by natural precursor clove and their functionalization with amine group. *J. Nanopart.*
983 *Res.* **2010**, *12* (5), 1667-1675.
- 984 108. Jeong, Y. I.; Kim, D. H.; Chung, K. D.; Kim, Y. H.; Lee, Y. S.; Choi, K. C., Antitumor
985 activity of trigonelline-incorporated chitosan nanoparticles. *J. Nanosci. Nanotechnol.* **2014**, *14* (8),
986 5633-5637.

- 987 109. Liu, L.; Wei, T.; Guan, X.; Zi, X.; He, H.; Dai, H., Size and morphology adjustment of PVP-
988 stabilized silver and gold nanocrystals synthesized by hydrodynamic assisted self-assembly. *J. Phys.*
989 *Chem. C* **2009**, *113*, 8595-8600.
- 990 110. Tsuji, M.; Gomi, S.; Maeda, Y.; Matsunaga, M.; Hikino, S.; Uto, K.; Tsuji, T.; Kawazumi, H.,
991 Rapid transformation from spherical nanoparticles, nanorods, cubes, or bipyramids to triangular
992 prisms of silver with PVP, citrate, and H₂O₂. *Langmuir* **2012**, *28* (24), 8845-8861.
- 993 111. Kedia, A.; Kumar, P. S., Solvent-adaptable poly(vinylpyrrolidone) binding induced
994 anisotropic shape control of gold nanostructures. *J. Phys. Chem. C* **2012**, *116* (44), 23721-23728.
- 995 112. Kim, K.; Park, H. K.; Kim, N. H., Silver-particle-based surface-enhanced Raman scattering
996 spectroscopy for biomolecular sensing and recognition. *Langmuir* **2006**, *22* (7), 3421-3427.
- 997 113. Kuo, P. L.; Chen, C. C.; Jao, M. W., Effects of polymer micelles of alkylated
998 polyethylenimines on generation of gold nanoparticles. *J. Phys. Chem. B* **2005**, *109* (19), 9445-9450.
- 999 114. Khan, Z.; Al-Nowaiser, F. M., Effect of poly(vinyl alcohol) on the size, shape, and rate of
1000 silver nanoparticles formation. *J. Disper. Sci. Technol.* **2011**, *32* (11), 1655-1660.
- 1001 115. Chang, W. G.; Shen, Y. H.; Xie, A. J.; Liu, X., Facile controlled synthesis of
1002 micro/nanostructure MCrO₄ (M = Ba, Pb) by using Gemini surfactant C₁₂-PEG-C₁₂ as a soft template.
1003 *Appl. Surf. Sci.* **2010**, *256* (13), 4292-4298.
- 1004 116. Yeap, S. P.; Toh, P. Y.; Ahmad, A. L.; Low, S. C.; Majetich, S. A.; Lim, J., Colloidal stability
1005 and magnetophoresis of gold-coated iron oxide nanorods in biological media. *J. Phys. Chem. C* **2012**,
1006 *116* (42), 22561-22569.
- 1007 117. Nguyen, T. D.; Mrabet, D.; Vu, T. T. D.; Dinh, C. T.; Do, T. O., Biomolecule-assisted route
1008 for shape-controlled synthesis of single-crystalline MnWO₄ nanoparticles and spontaneous assembly
1009 of polypeptide-stabilized mesocrystal microspheres. *Cryst. Eng. Comm.* **2011**, *13* (5), 1450-1460.
- 1010 118. Becker, R.; Liedberg, B.; Kall, P. O., CTAB promoted synthesis of Au nanorods -
1011 Temperature effects and stability considerations. *J. Colloid Interf. Sci.* **2010**, *343* (1), 25-30.
- 1012 119. Zhang, Y. J.; Du, Y. P.; Xu, H. R.; Wang, Q. B., Diverse-shaped iron sulfide nanostructures
1013 synthesized from a single source precursor approach. *Cryst. Eng. Comm.* **2010**, *12* (11), 3658-3663.
- 1014 120. Song, X. C.; Zhao, Y.; Zheng, Y. F.; Yang, E.; Fu, J.; He, Y., Fabrication of Ag/C coaxial
1015 nanocables with cross-linked structure by SDS-assisted hydrothermal approach. *Cryst. Growth Des.*
1016 **2008**, *8* (6), 1823-1826.
- 1017 121. Kim, J.; Hong, S.; Jang, H. J.; Choi, Y.; Park, S., Influence of iodide ions on morphology of
1018 silver growth on gold hexagonal nanoplates. *J. Colloid Interf. Sci.* **2013**, *389*, 71-76.
- 1019 122. Tsuji, M.; Miyamae, N.; Hashimoto, M.; Nishio, M.; Hikino, S.; Ishigami, N.; Tanaka, I.,
1020 Shape and size controlled synthesis of gold nanocrystals using oxidative etching by AuCl₄⁻ and Cl⁻
1021 anions in microwave-polyol process. *Colloid Surf. A* **2007**, *302* (1-3), 587-598.
- 1022 123. Sau, T. K.; Murphy, C. J., Role of ions in the colloidal synthesis of gold nanowires. *Philos.*

- 1023 *Mag.* **2007**, *87* (14-15), 2143-2158.
- 1024 124. Seo, D.; Park, J. C.; Song, H., Polyhedral gold nanocrystals with O_h symmetry: From
1025 octahedra to cubes. *J. Am. Chem. Soc.* **2006**, *128* (46), 14863-14870.
- 1026 125. Tsuji, M.; Matsuo, R.; Jiang, P.; Miyamae, N.; Ueyama, D.; Nishio, M.; Hikino, S.; Kumagae,
1027 H.; Kamarudin, K. S. N.; Tang, X. L., Shape-dependent evolution of Au@Ag core-shell nanocrystals
1028 by PVP-assisted N,N-dimethylformamide reduction. *Cryst. Growth Des.* **2008**, *8* (7), 2528-2536.
- 1029 126. Long, N. V.; Chien, N. D.; Hirata, H.; Matsubara, T.; Ohtaki, M.; Nogami, M., Highly
1030 monodisperse cubic and octahedral rhodium nanocrystals: Their evolutions from sharp polyhedrons
1031 into branched nanostructures and surface-enhanced Raman scattering. *J. Cryst. Growth* **2011**, *320* (1),
1032 78-89.
- 1033 127. Jiu, J. T.; Sukanuma, K.; Nogi, M., Effect of additives on the morphology of single-crystal
1034 Au nanosheet synthesized using the polyol process. *J. Mater. Sci.* **2011**, *46* (14), 4964-4970.
- 1035 128. Wang, C. H.; Zhang, X. T.; Zhang, Y. L.; Jia, Y.; Yuan, B.; Yang, J. K.; Sun, P. P.; Liu, Y. C.,
1036 Morphologically-tunable TiO_2 nanorod film with high energy facets: green synthesis, growth
1037 mechanism and photocatalytic activity. *Nanoscale* **2012**, *4* (16), 5023-5030.
- 1038 129. Zhang, X. Y.; Wang, M. Q.; Ding, J. J., Shape-selective synthesis, characterization and
1039 upconversion improvement of Yb^{3+}/Er^{3+} doped $LiYF_4$ microphosphors through pH tuning. *RSC Adv.*
1040 **2014**, *4* (55), 29165-29172.
- 1041 130. Si, S.; Leduc, C.; Delville, M. H.; Lounis, B., Short gold nanorod growth revisited: The
1042 critical role of the bromide counterion. *Chem. Phys. Chem.* **2012**, *13* (1), 193-202.
- 1043 131. Zhang, J. H.; Liu, H. Y.; Wang, Z. L.; Ming, N. B., Synthesis of gold regular octahedra with
1044 controlled size and plasmon resonance. *Appl. Phys. Lett.* **2007**, *90* (16), 163122.
- 1045 132. Sun, X.; Zhang, Y. W.; Du, Y. P.; Yan, Z. G.; Si, R.; You, L. P.; Yan, C. H., From
1046 trifluoroacetate complex precursors to monodisperse rare-earth fluoride and oxyfluoride nanocrystals
1047 with diverse shapes through controlled fluorination in solution phase. *Chem. Eur. J.* **2007**, *13* (8),
1048 2320-2332.
- 1049 133. Gao, D. L.; Gao, W.; Shi, P.; Li, L., pH- and surfactant-mediated tunable morphology and
1050 upconversion of rare-earth doped fluoride microcrystals. *RSC Adv.* **2013**, *3* (34), 14757-14765.
- 1051 134. Shinde, V. R.; Gujar, T. P.; Noda, T.; Fujita, D.; Vinu, A.; Grandcolas, M.; Ye, J. H., Growth
1052 of shape- and size-selective zinc oxide nanorods by a microwave-assisted chemical bath deposition
1053 method: Effect on photocatalysis properties. *Chem. Eur. J.* **2010**, *16* (34), 10569-10575.
- 1054 135. Fan, F. R.; Ding, Y.; Liu, D. Y.; Tian, Z. Q.; Wang, Z. L., Facet-selective epitaxial growth of
1055 heterogeneous nanostructures of semiconductor and metal: ZnO nanorods on Ag nanocrystals. *J. Am.*
1056 *Chem. Soc.* **2009**, *131* (34), 12036-12037.
- 1057 136. Cathcart, N.; Kitaev, V., Multifaceted prismatic silver nanoparticles: synthesis by chloride-
1058 directed selective growth from thiolate-protected clusters and SERS properties. *Nanoscale* **2012**, *4*

- 1059 (22), 6981-6989.
- 1060 137. Sayed, S. Y.; Wang, F.; Malac, M.; Li, P.; Wang, D.; Buriak, J., Preferential face deposition of
1061 gold nanoparticles on silicon nanowires by galvanic displacement. *Cryst. Eng. Comm.* **2012**, *14* (16),
1062 5230-5234.
- 1063 138. Lim, B.; Camargo, P. H. C.; Xia, Y. N., Mechanistic study of the synthesis of an
1064 nanotadpoles, nanokites, and microplates by reducing aqueous H₂AuCl₄ with poly(vinyl pyrrolidone).
1065 *Langmuir* **2008**, *24* (18), 10437-10442.
- 1066 139. Wang, G. Z.; Shen, X. S.; Hong, X.; Zhu, W., Nanospheres of silver nanoparticles:
1067 agglomeration, surface morphology control and application as SERS substrates. *Phys. Chem. Chem.*
1068 *Phys.* **2009**, *11* (34), 7450-7454.
- 1069 140. Jana, N. R.; Gearheart, L.; Murphy, C. J., Seed-mediated growth approach for shape-
1070 controlled synthesis of spheroidal and rod-like gold nanoparticles using a surfactant template. *Adv.*
1071 *Mater.* **2001**, *13* (18), 1389-1393.
- 1072 141. Song, R. Q.; Colfen, H., Additive controlled crystallization. *Cryst. Eng. Comm.* **2011**, *13* (5),
1073 1249-1276.
- 1074 142. Ringe, E.; Van Duyne, R. P.; Marks, L. D., Wulff construction for alloy nanoparticles. *Nano*
1075 *Lett.* **2011**, *11* (8), 3399-3403.
- 1076 143. Ha, T. H.; Koo, H. J.; Chung, B. H., Shape-controlled syntheses of gold nanoprisms and
1077 nanorods influenced by specific adsorption of halide ions. *J. Phys. Chem. C* **2007**, *111* (3), 1123-1130.
- 1078 144. Kirowa-Eisner, E.; Bonfil, Y.; Tzur, D.; Gileadi, E., Thermodynamics and kinetics of upd of
1079 lead on polycrystalline silver and gold. *J. Electroanal. Chem.* **2003**, *552*, 171-183.
- 1080 145. Beni, V.; Newton, H. V.; Arrigan, D. W. M.; Hill, M.; Lane, W. A.; Mathewson, A.,
1081 Voltammetric behaviour at gold electrodes immersed in the BCR sequential extraction scheme media -
1082 Application of underpotential deposition-stripping voltammetry to determination of copper in soil
1083 extracts. *Anal. Chim. Acta.* **2004**, *502* (2), 195-206.
- 1084 146. Jiang, L. P.; Xu, S.; Zhu, J. M.; Zhang, J. R.; Zhu, J. J.; Chen, H. Y., Ultrasonic-assisted
1085 synthesis of monodisperse single-crystalline silver nanoplates and gold nanorings. *Inorg. Chem.* **2004**,
1086 *43* (19), 5877-5883.
- 1087 147. Personick, M. L.; Langille, M. R.; Zhang, J.; Mirkin, C. A., Shape control of gold
1088 nanoparticles by silver underpotential deposition. *Nano Lett.* **2011**, *11* (8), 3394-3398.
- 1089 148. Price, S. W. T.; Speed, J. D.; Kannan, P.; Russell, A. E., Exploring the first steps in core-shell
1090 electrocatalyst preparation: In situ characterization of the underpotential deposition of Cu on
1091 supported Au nanoparticles. *J. Am. Chem. Soc.* **2011**, *133* (48), 19448-19458.
- 1092 149. Yu, Y.; Zhang, Q. B.; Xie, J. P.; Lee, J. Y., Engineering the architectural diversity of
1093 heterogeneous metallic nanocrystals. *Nat. Commun.* **2013**, *4*, 1454.
- 1094 150. Langille, M. R.; Personick, M. L.; Zhang, J.; Mirkin, C. A., Defining rules for the shape

- 1095 evolution of gold nanoparticles. *J. Am. Chem. Soc.* **2012**, *134* (35), 14542-14554.
- 1096 151. Joo, S. H.; Park, J. Y.; Tsung, C. K.; Yamada, Y.; Yang, P. D.; Somorjai, G. A., Thermally
1097 stable Pt/mesoporous silica core-shell nanocatalysts for high-temperature reactions. *Nat. Mater.* **2009**,
1098 *8* (2), 126-131.
- 1099 152. Li, D.; Kaner, R. B., Shape and aggregation control of nanoparticles: Not shaken, not stirred.
1100 *J. Am. Chem. Soc.* **2006**, *128* (3), 968-975.
- 1101 153. Piao, Y. K., J. Na, H. B. Kim, D. Baek, J. S. Ko, M. K. Lee, J. H. Shokouhimehr, M. Hyeon,
1102 T., Wrap-bake-peel process for nanostructural transformation from β -FeOOH nanorods to
1103 biocompatible iron oxide nanocapsules. *Nat. Mater.* **2008**, *7* (3), 242-247.
- 1104 154. Lee, H., Utilization of shape-controlled nanoparticles as catalysts with enhanced activity and
1105 selectivity. *Rsc Adv.* **2014**, *4* (77), 41017-41027.
- 1106 155. Yao, T.; Liu, S. J.; Sun, Z. H.; Li, Y. Y.; He, S.; Cheng, H.; Xie, Y.; Liu, Q. H.; Jiang, Y.; Wu,
1107 Z. Y.; Pan, Z. Y.; Yan, W. S.; Wei, S. Q., Probing nucleation pathways for morphological manipulation
1108 of platinum nanocrystals. *J. Am. Chem. Soc.* **2012**, *134* (22), 9410-9416.
- 1109 156. Ming, H.; Torad, N. L. K.; Chiang, Y. D.; Wu, K. C. W.; Yamauchi, Y., Size- and shape-
1110 controlled synthesis of Prussian Blue nanoparticles by a polyvinylpyrrolidone-assisted crystallization
1111 process. *Cryst. Eng. Comm.* **2012**, *14* (10), 3387-3396.
- 1112 157. Liu, Z.; Lv, B. L.; Wu, D.; Sun, Y. H., Morphology and magnetic properties of α -Fe₂O₃
1113 particles prepared by octadecylamine-assisted hydrothermal method. *Particuology* **2012**, *10* (4), 456-
1114 461.
- 1115 158. Tsuji, M.; Alam, M. J.; Matsunaga, M.; Yamaguchi, D., Shape changes in Au-Ag bimetallic
1116 systems involving polygonal Au nanocrystals to spherical Au/Ag alloy and excentered Au core Ag/Au
1117 alloy shell particles under oil-bath heating. *Cryst. Eng. Comm.* **2011**, *13* (8), 2984-2993.
- 1118 159. Long, N. V.; Chien, N. D.; Hayakawa, T.; Matsubara, T.; Ohtaki, M.; Nogami, M., Sharp
1119 cubic and octahedral morphologies of poly(vinylpyrrolidone)-stabilised platinum nanoparticles by
1120 polyol method in ethylene glycol: their nucleation, growth and formation mechanisms. *J. Exp.*
1121 *Nanosci.* **2012**, *7* (2), 133-149.
- 1122 160. J.C. Masy, M. C., Using a turbidimetric method to study the kinetics of agglomeration of
1123 potassium sulphate in a liquid medium. *Chem. Eng. Sci.* **1991**, *46* (2), 693-701.
- 1124 161. Zhongli Wang, X. L., Minfeng Lv, Ping Chai, Yao Liu, and Jian Meng, Preparation of ferrite
1125 MFe₂O₄ (M= Co, Ni) ribbons with nanoporous structure and their magnetic properties. *J. Phys. Chem.*
1126 *B* **2008**, *112*, 11292-11297.
- 1127 162. Mikami, T.; Sakuma, T.; Hirasawa, I., CSD-controlled reactive crystallization of SrSO₄ in the
1128 presence of polyethylenimine. *Chem. Eng. Res. Des.* **2010**, *88* (9A), 1200-1205.
- 1129 163. Jung, T.; Kim, W. S.; Choi, C. K., Effect of monovalent salts on morphology of calcium
1130 carbonate crystallized in Couette-Taylor reactor. *Cryst. Res. Technol.* **2005**, *40* (6), 586-592.

- 1131 164. Wang, G. Z.; Saeterli, R.; Rorvik, P. M.; van Helvoort, A. T. J.; Holmestad, R.; Grande, T.;
1132 Einarsrud, M. A., Self-assembled growth of PbTiO₃ nanoparticles into microspheres and bur-like
1133 structures. *Chem. Mater.* **2007**, *19* (9), 2213-2221.
- 1134 165. Olderoy, M. O.; Xie, M. L.; Strand, B. L.; Flaten, E. M.; Sikorski, P.; Andreassen, J. P.,
1135 Growth and nucleation of calcium carbonate vaterite crystals in presence of alginate. *Cryst. Growth*
1136 *Des.* **2009**, *9* (12), 5176-5183.
- 1137 166. Kim, J. M.; Chang, S. M.; Chang, J. H.; Kim, W. S., Agglomeration of
1138 nickel/cobalt/manganese hydroxide crystals in Couette-Taylor crystallizer. *Colloid Surf. A* **2011**, *384*
1139 (1-3), 31-39.
- 1140 167. Wang, S. F.; Gu, F.; Li, C. Z.; Cao, H. M., Shape-controlled synthesis of CeOHCO₃ and
1141 CeO₂ microstructures. *J. Cryst. Growth* **2007**, *307* (2), 386-394.
- 1142 168. Kim, Q.-P. M. a. W.-S., Agglomeration of Ni-Rich hydroxide in reaction crystallization:
1143 Effect of taylor vortex dimension and intensity. *Cryst. Growth Des.* **2015**, *15* (4), 1726-1734.
- 1144 169. Penn, R. L.; Banfield, J. F., Imperfect oriented attachment: Dislocation generation in defect-
1145 free nanocrystals. *Science* **1998**, *281* (5379), 969-971.
- 1146 170. Zhang, J.; Huang, F.; Lin, Z., Progress of nanocrystalline growth kinetics based on oriented
1147 attachment. *Nanoscale* **2010**, *2* (1), 18-34.
- 1148 171. Munoz-Rojas, D.; Oro-Sole, J.; Gomez-Romero, P., From nanosnakes to nanosheets: A
1149 matrix-mediated shape evolution. *J. Phys. Chem. C* **2008**, *112* (51), 20312-20318.
- 1150 172. Lee, E. J. H.; Ribeiro, C.; Longo, E.; Leite, E. R., Oriented attachment: An effective
1151 mechanism in the formation of anisotropic nanocrystals. *J. Phys. Chem. B* **2005**, *109* (44), 20842-
1152 20846.
- 1153 173. Li, D.; Nielsen, M. H.; Lee, J. R.; Frandsen, C.; Banfield, J. F.; De Yoreo, J. J., Direction-
1154 specific interactions control crystal growth by oriented attachment. *Science* **2012**, *336* (6084), 1014-
1155 1018.
- 1156 174. Zhang, D. F.; Zhang, Q.; Niu, L. Y.; Jiang, L.; Yin, P. G.; Guo, L., Self-assembly of gold
1157 nanoparticles into chain-like structures and their optical properties. *J. Nanopart. Res.* **2011**, *13* (9),
1158 3923-3928.
- 1159 175. Tsao, C. S.; Chuang, C. M.; Chen, C. Y.; Huang, Y. C.; Cha, H. C.; Hsu, F. H.; Chen, C. Y.;
1160 Tu, Y. C.; Su, W. F., Reaction kinetics and formation mechanism of TiO₂ nanorods in solution: An
1161 insight into oriented attachment. *J. Phys. Chem. C* **2014**, *118* (45), 26332-26340.
- 1162 176. Zhou, W. W.; Yan, B.; Cheng, C. W.; Cong, C. X.; Hu, H. L.; Fan, H. J.; Yu, T., Facile
1163 synthesis and shape evolution of highly symmetric 26-facet polyhedral microcrystals of Cu₂O. *Cryst.*
1164 *Eng. Comm.* **2009**, *11* (11), 2291-2296.
- 1165 177. Whitesides, G. M.; Grzybowski, B., Self-assembly at all scales. *Science* **2002**, *295* (5564),
1166 2418-2421.

- 1167 178. Si, R.; Zhang, Y. W.; Zhou, H. P.; Sun, L. D.; Yan, C. H., Controlled-synthesis, self-assembly
1168 behavior, and surface-dependent optical properties of high-quality rare-earth oxide nanocrystals.
1169 *Chem. Mater.* **2007**, *19* (1), 18-27.
- 1170 179. Lee, J. Y.; Zhang, Q. B.; Xie, J. P.; Yang, J. H., Monodisperse icosahedral Ag, Au, and Pd
1171 nanoparticles: Size control strategy and superlattice formation. *ACS Nano* **2009**, *3* (1), 139-148.
- 1172 180. Knecht, M. R.; Sethi, M.; Joung, G., Linear assembly of Au nanorods using biomimetic
1173 ligands. *Langmuir* **2009**, *25* (3), 1572-1581.
- 1174 181. Nguyen, T. D.; Jankowski, E.; Glotzer, S. C., Self-assembly and reconfigurability of shape-
1175 shifting particles. *ACS Nano* **2011**, *5* (11), 8892-8903.
- 1176 182. Nikoobakht, B.; Wang, Z. L.; El-Sayed, M. A., Self-assembly of gold nanorods. *J. Phys.*
1177 *Chem. B* **2000**, *104* (36), 8635-8640.
- 1178 183. Tian, Z. S.; Xu, C. X.; Li, J. T.; Zhu, G. Y.; Xu, X. Y.; Dai, J.; Shi, Z. L.; Lin, Y., Manganese
1179 ion-assisted assembly of superparamagnetic graphene oxide microbowls. *Appl. Phys. Lett.* **2014**, *104*
1180 (12), 121602.
- 1181 184. Wang, J. J.; Chen, Y. G.; Liu, H.; Li, R. Y.; Sun, X. L., Synthesis of Pd nanowire networks by
1182 a simple template-free and surfactant-free method and their application in formic acid
1183 electrooxidation. *Electrochem. Commun.* **2010**, *12* (2), 219-222.
- 1184 185. Kooij, E. S.; Ahmed, W.; Laarman, R. P. B.; Hellenthal, C.; van Silfhout, A.; Poelsema, B.,
1185 Dipole directed ring assembly of Ni-coated Au-nanorods. *Chem. Commun.* **2010**, *46* (36), 6711-6713.
- 1186 186. Deng, D. W.; Qin, Y. B.; Yang, X.; Yu, J. S.; Pan, Y., The selective synthesis of water-soluble
1187 highly luminescent CdTe nanoparticles and nanorods: The influence of the precursor Cd/Te molar
1188 ratio. *J. Cryst. Growth* **2006**, *296* (2), 141-149.
- 1189 187. Orendorff, C. J.; Hankins, P. L.; Murphy, C. J., pH-triggered assembly of gold nanorods.
1190 *Langmuir* **2005**, *21* (5), 2022-2026.
- 1191 188. Kumacheva, E.; Zhao, N.; Liu, K.; Greener, J.; Nie, Z. H., Close-packed superlattices of
1192 side-by-side assembled Au-CdSe nanorods. *Nano Lett.* **2009**, *9* (8), 3077-3081.
- 1193 189. Ostwald, W., Über die vermeintliche Isomerie des roten und gelben Quecksilberoxyds und
1194 die Oberflächenspannung fester Körper. *Z. Phys. Chem.* **1900**, *34*, 495.
- 1195 190. Noorduyn, W. L.; Vlieg, E.; Kellogg, R. M.; Kaptein, B., From Ostwald ripening to single
1196 chirality. *Angew. Chem. Int. Ed.* **2009**, *48* (51), 9600-9606.
- 1197 191. Luna, C.; Barriga-Castro, E. D.; Mendoza-Resendez, R., The effects of aging time on the
1198 size, morphology, oriented attachment and magnetic behavior of hematite nanocrystals synthesized by
1199 forced hydrolysis of Fe-III solutions. *Acta. Mater.* **2014**, *66*, 405-413.
- 1200 192. Senapati, D.; Singh, A. K.; Khan, S. A.; Senapati, T.; Ray, P. C., Probing real time gold
1201 nanostar formation process using two-photon scattering spectroscopy. *Chem. Phys. Lett.* **2011**, *504* (1-
1202 3), 46-51.

- 1203 193. Peretyazhko, T. S.; Zhang, Q. B.; Colvin, V. L., Size-controlled dissolution of silver
1204 nanoparticles at neutral and acidic pH conditions: kinetics and size changes. *Environ. Sci. Technol.*
1205 **2014**, *48* (20), 11954-11961.
- 1206 194. Qu, X. F.; Yao, Q. Z.; Zhou, G. T.; Fu, S. Q.; Huang, J. L., Formation of hollow magnetite
1207 microspheres and their evolution into durian-like architectures. *J. Phys. Chem. C* **2010**, *114*(19), 8734-
1208 8740.
- 1209 195. Guan N., W. Y., Sun D., Xu, J., A simple one-pot synthesis of single-crystalline magnetite
1210 hollow spheres from a single iron precursor. *Nanotechnology* **2009**, *20* (10), 105603.
- 1211 196. Chen, J. S.; Li, C. M.; Zhou, W. W.; Yan, Q. Y.; Archer, L.A.; and Lou, X. W. One-pot
1212 formation of SnO₂ hollow nanospheres and α -Fe₂O₃@SnO₂ nanorattles with large void space and their
1213 lithium storage properties. *Nanoscale* **2009**, *1*, 280-285.
- 1214 197. Bewernitz, M. A.; Gebauer, D.; Long, J.; Colfen, H.; Gower, L. B., A metastable liquid
1215 precursor phase of calcium carbonate and its interactions with polyaspartate. *Faraday Discuss.* **2012**,
1216 *159*, 291-312.
- 1217 198. Shoji, M.; Eto, T.; Takiyama, H., A kinetic study of the influence of modulated
1218 undersaturation operation on crystal size distribution in cooling-type batch crystallization. *J. Chem.*
1219 *Eng. Jpn.* **2011**, *44* (3), 191-196.
- 1220 199. O'Ciardha, C. T.; Hutton, K. W.; Mitchell, N. A.; Frawley, P. J., Simultaneous parameter
1221 estimation and optimization of a seeded antisolvent crystallization. *Cryst. Growth Des.* **2012**, *12* (11),
1222 5247-5261.
- 1223
- 1224

Figures

1225

1226

1227 **Figure 1.** Typical morphology of solid and mesoporous/hollow inorganic nanoparticles with the
1228 shapes of 0D, 1D, 2D and other 3D complex structure.

1229

Figure 2. Schematic illustration of Free energy diagram for nucleation.

1230

Figure 3. Diffusion-reaction model for crystals growth with concentration driving in solution state.

1231

1232 **Figure 4.** Scheme of LaMer theory for nucleation and growth and the variation of particles number
1233 during the nucleation and growth process.

1233

1234 **Figure 5.** Schematic illustration of well-facted polyhedral Au nanoparticles changing with
1235 concentration of reductant by SEM images. (Reprinted from ref. 64, Copyright (2012) with
1236 permission from the American Chemical Society.)

1236

1237 **Figure 6.** Schematic illustration for the self-assembly of two kinds of α -Fe₂O₃ dendrites by altering
1238 pH of bulk solution and their corresponding TEM images. (Reprinted from ref. 74, Copyright (2006)
1239 with permission from the Elsevier B.V.)

1239

1240 **Figure 7.** Representative TEM images of Rh nanoparticles synthesized using ethylene glycol,
1241 diethylene glycol, triethylene glycol, and tetraethylene glycol solvents with the reagents (a-d)
1242 Rh₂(TFA)₄, (e-h) RhBr₃, and (i-l) RhCl₃ (TFA = trifluoroacetate). Outlined images indicate the set of
1243 reaction conditions which results in the most monodisperse yield of Rh icosahedra (red), cubes
1244 (green), and triangular plates (blue). Scale bars are 20 nm. (Reprinted from ref. 82, Copyright (2011)
1245 with permission from the American Chemical Society.)

1245

1246 **Figure 8.** Schematic illustration of temperature variation process for evolution of Au plates and SEM
1247 images. (Reprinted from ref. 85, Copyright (2011) with permission from the Elsevier B.V.)

1247

1248 **Figure 9.** (a) Schematic illustrating the relationship between the geometry and bounding crystal facets
1249 (colorized) of the wurtzite CdSe nanocrystal seeds and the nanocrystals produced in the seed-
1250 mediated synthesis. Typical TEM images of wz-CdSe nanocrystals with shapes of (b) hexagonal
1251 platelets, (c) cubes, and (d) rods. (e) TEM image from a similar synthesis conducted without using the

1251 CdSe nanocrystal seeds, resulting in elongated and misshapen particles. The scale bars each
1252 correspond to 50 nm. (Reprinted from ref. 100, Copyright (2013) with permission from the American
1253 Chemical Society.)

1254 **Figure 10.** Schematic of additive/surfactants for the shape control of inorganic nanoparticles with
1255 selective adsorption.

1256 **Figure 11.** (a)-(e) Morphology evolution of Au nanocrystals synthesized in the presence of Ag(I) and
1257 Pd(II) foreign Ions in a mediated polyol process. (Reprinted from ref. 12, Copyright (2011) with
1258 permission from the American Chemical Society.)

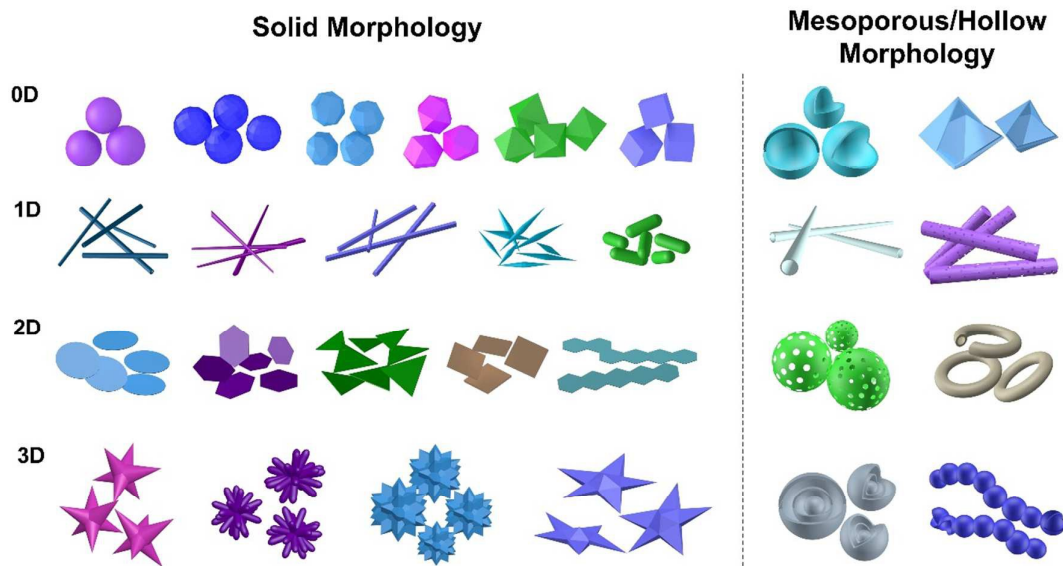
1259 **Figure 12.** Schematic illustration of mechanism difference in (a) aggregation, and (b) agglomeration.

1260 **Figure 13.** Sequence of images showing typical dynamics of the attachment process (A to G). The
1261 surfaces of particles I and II made transient contact at many points and orientations (points 1-1, 1-2, 2-
1262 3, and 3-4) before finally attaching and growing together (points 3-5). (H) High-resolution image of
1263 interface in (G) showing twin structure (an inclined twin plane). The yellow dashed line in (G) shows
1264 the original boundary of the attached particle. (I and J) High-resolution in situ TEM image (I) and fast
1265 Fourier transform (FFT) (J) of an interface from another OA event demonstrating formation of a (101)
1266 twin interface after attachment. The grain boundary is delineated by a dashed line in (I). Scale bars are
1267 5 nm for (A) to (G) (Reprinted from ref. 173, Copyright (2012) with permission from the American
1268 Association for the Advancement of Science.)

1269 **Figure 14.** Schematic illustration of Ostwald ripening process.

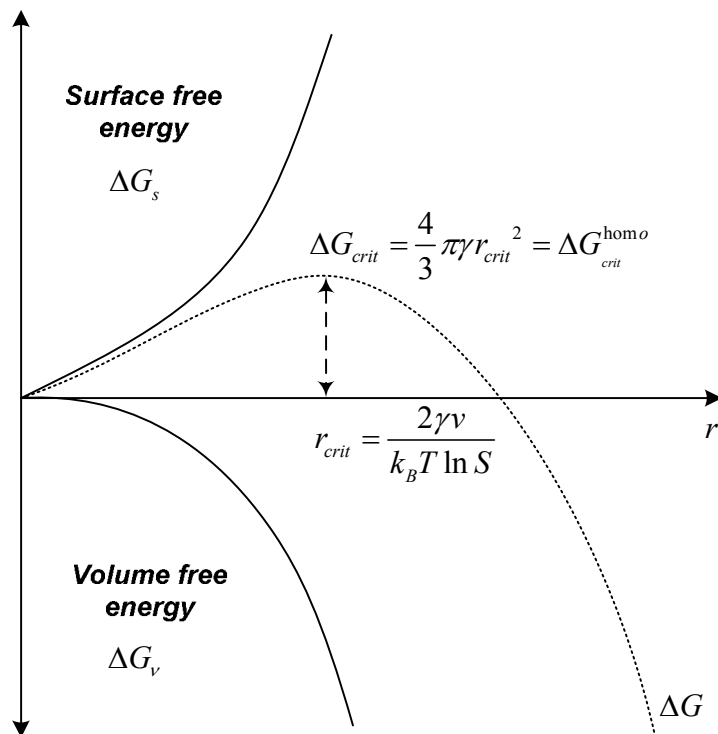
1270 **Figure 15.** (a) Schematic illustration of the formation of SnO₂ hollow nanospheres, (b) Schematic
1271 illustration of the formation of α -Fe₂O₃@SnO₂ nano-rattles, and the TEM images with time.
1272 (Reprinted from ref. 196, Copyright (2009) with permission from the Royal Society of Chemistry.)

1273

1274 **Figure 1.**

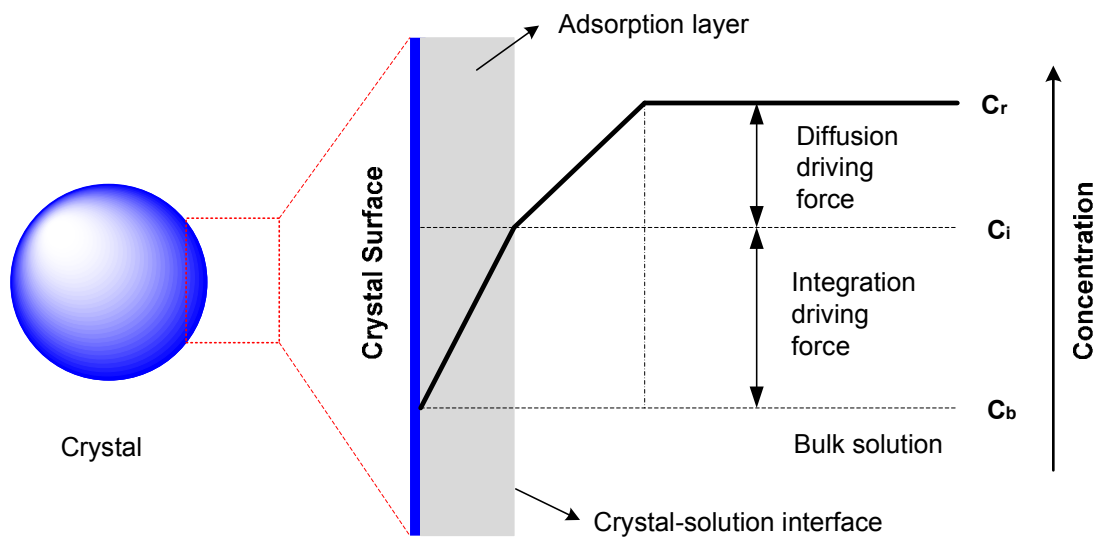
1275

1276

1277 **Figure 2.**

1278

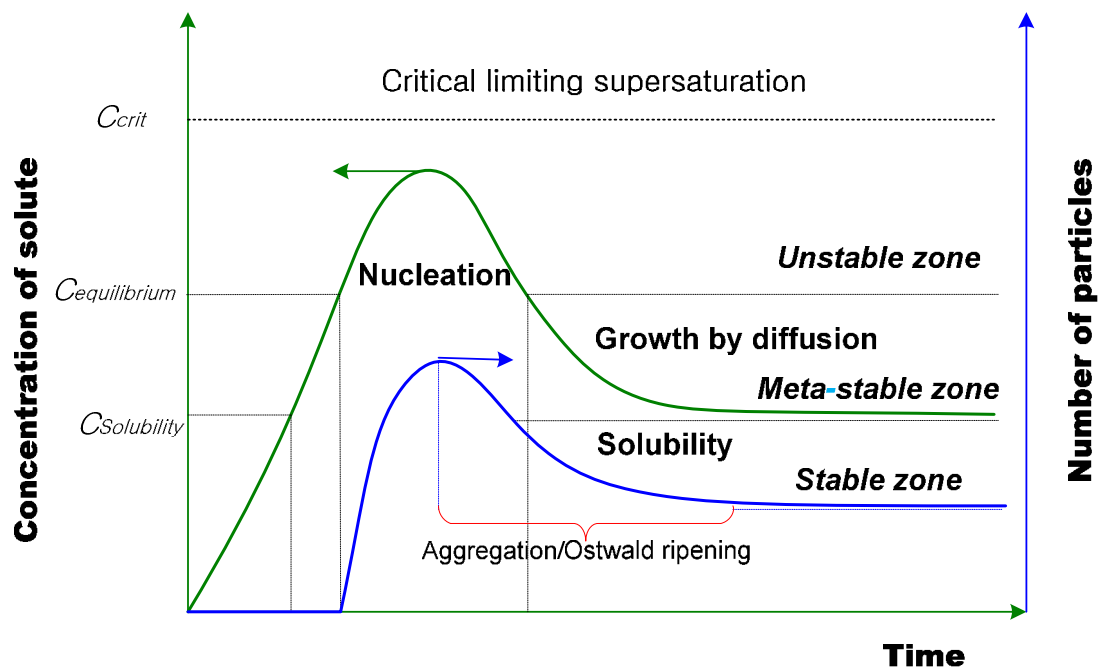
1279

1280 **Figure 3.**

1281

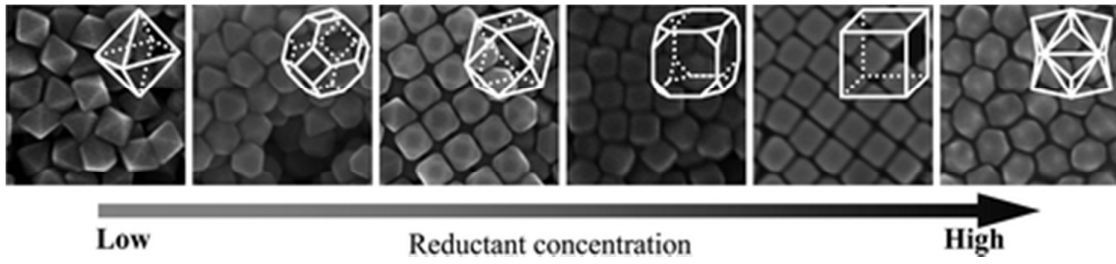
1282

1283 Figure 4.

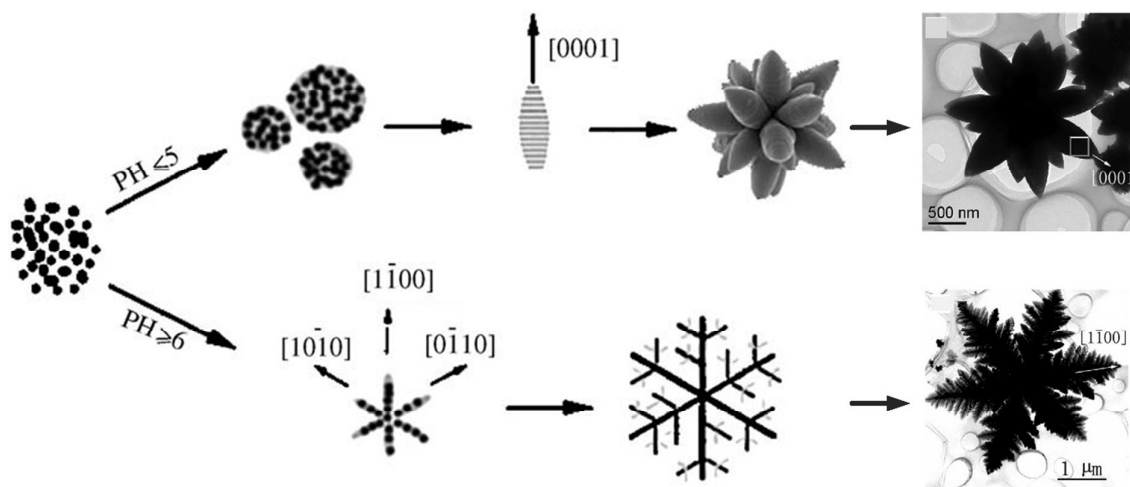


1284

1285

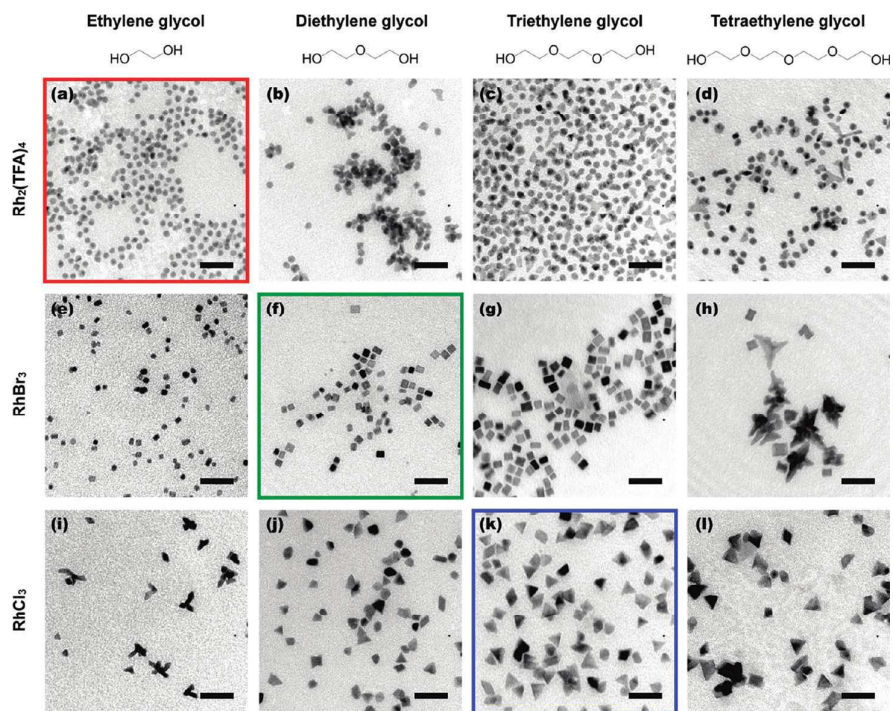
1286 **Figure 5.**

1288

1289 **Figure 6.**

1290

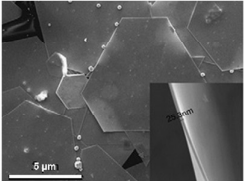
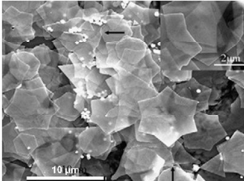
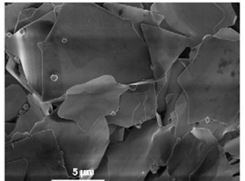
1291

1292 **Figure 7.**

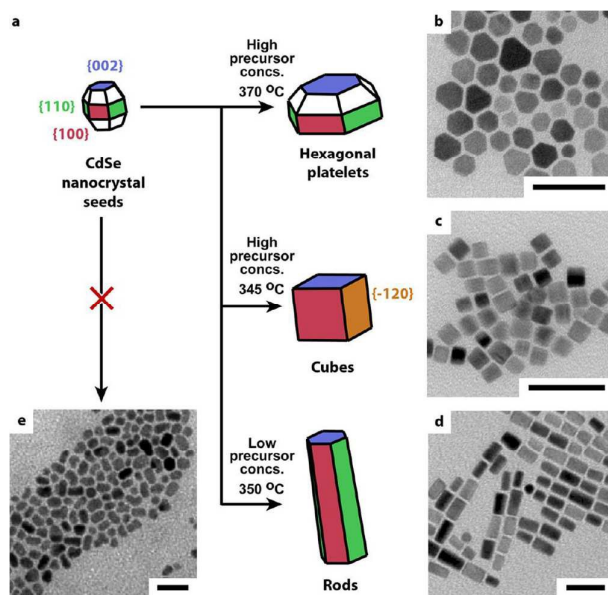
1293

1294

1295 **Figure 8.**

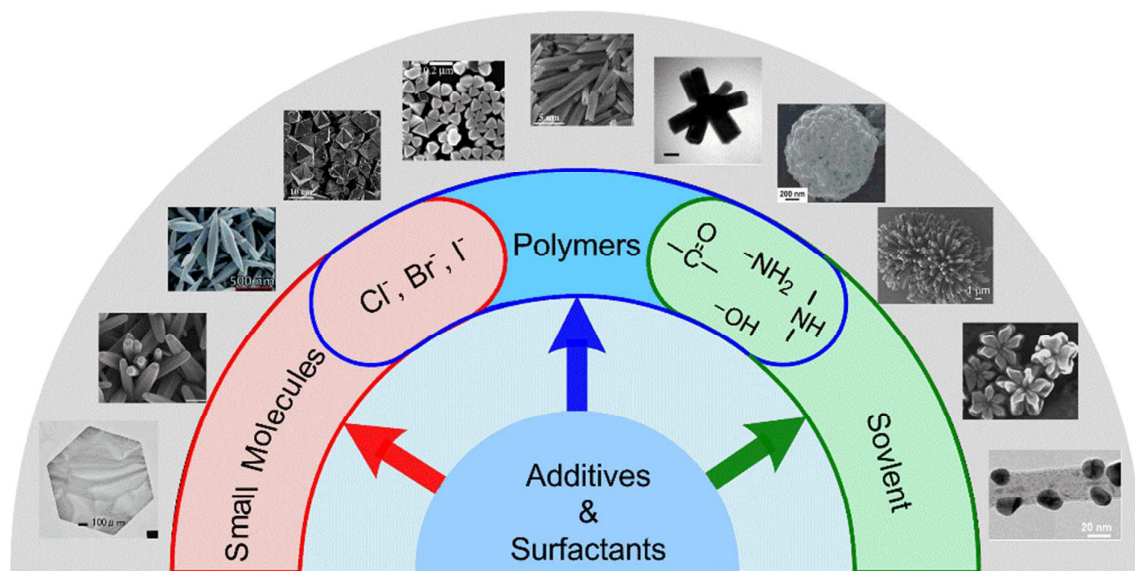
Forming Temperature	30 °C	20 °C	20 °C
Precipitating Temperature	30 °C	30 °C	50 °C
Corresponding SEM Image			

1296
1297

1298 **Figure 9.**

1299

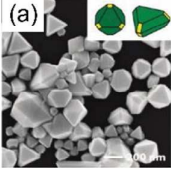
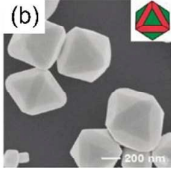
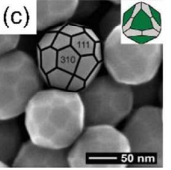
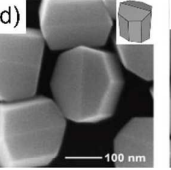
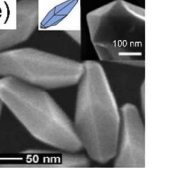
1300

1301 **Figure 10.**

1302

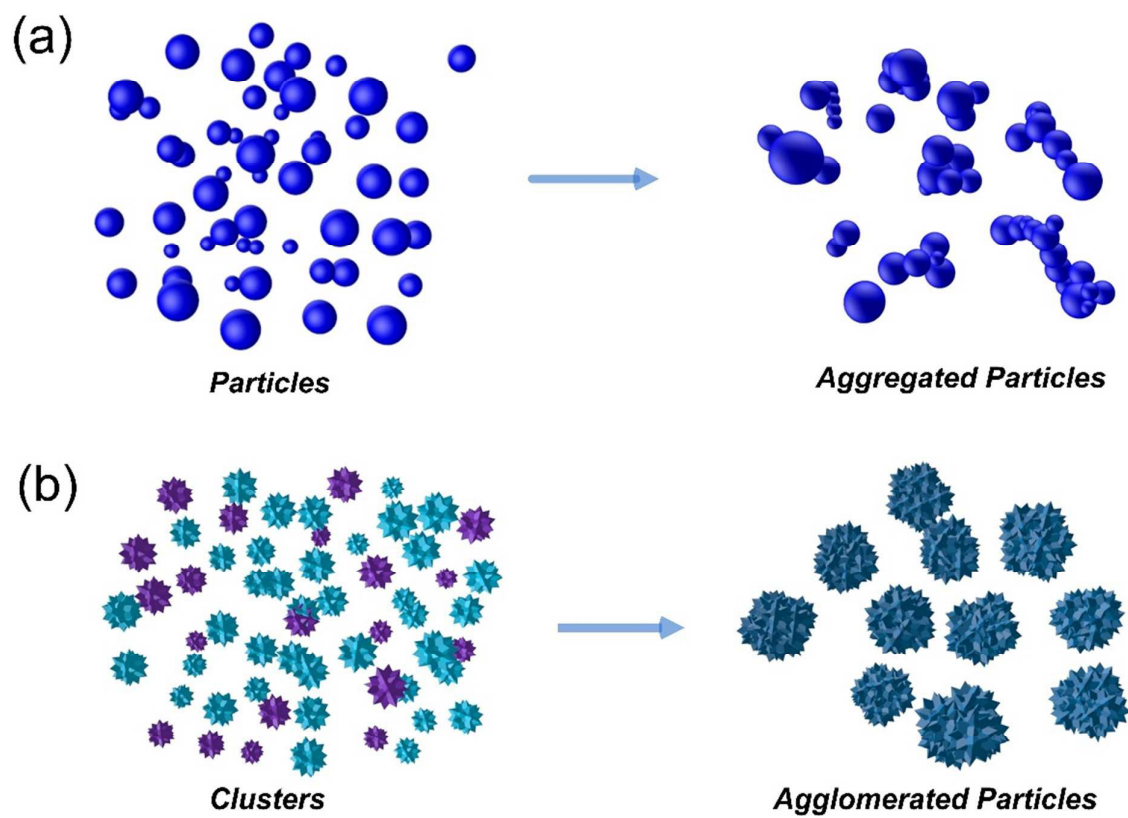
1303

1304 **Figure 11.**

Foreign ions	<i>Pd(II)</i> only	<i>Ag(II)</i> only	Low ratio of <i>Ag(I)/Pd(II)</i>	High ratio of <i>Ag(I)/Pd(II)</i>	Very high ratio of <i>Ag(I)/Pd(II)</i>
Shape of Au NPs & corresponding SEM images					
Main facets	{111}+{100}	{111}+{110}	{111}+{310}	{310}	

1305

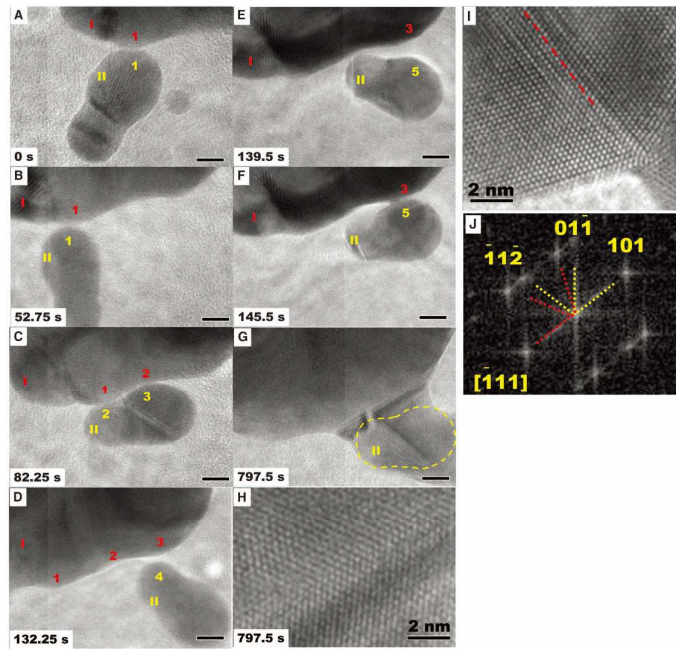
1306

1307 **Figure 12.**

1308

1309

1310 Figure 13.

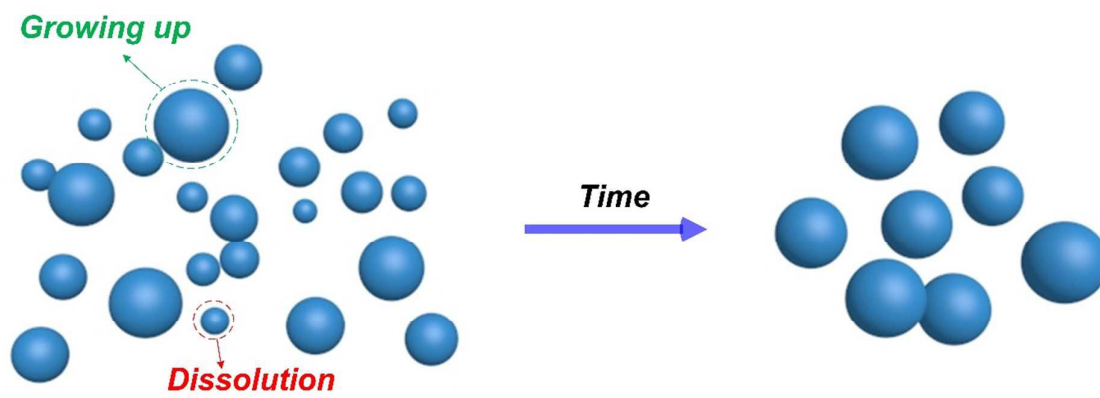


1311

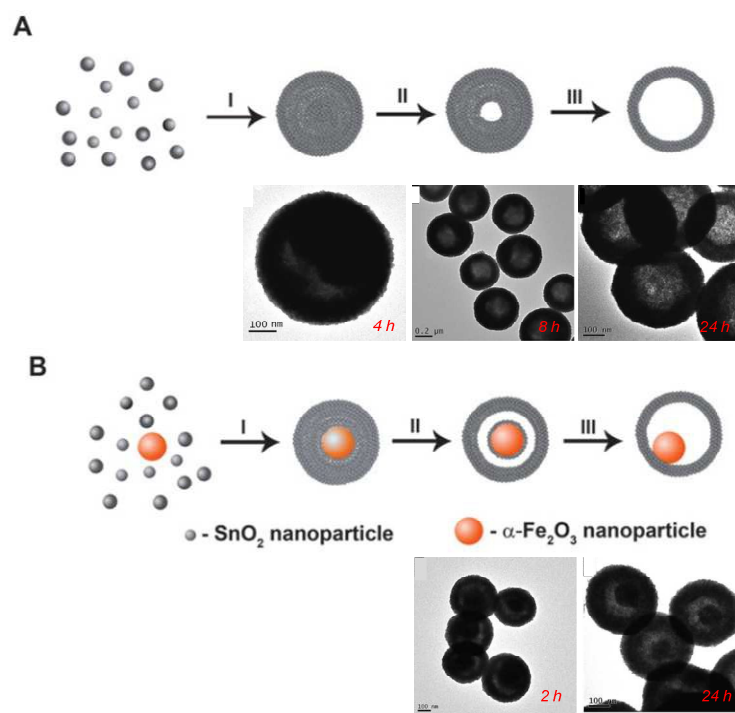
1312

1313 **Figure 14.**

1314



1315
1316

1317 **Figure 15.**

1318

1319